

## Article

# Modeling of Future Streamflow Hazards in Interior Alaska River Systems and Implications for Applied Planning

Alec P. Bennett <sup>1</sup>, Vladimir A. Alexeev <sup>2,\*</sup> and Peter A. Bieniek <sup>2</sup>

<sup>1</sup> College of Business & Security Management, University of Alaska Fairbanks, Fairbanks, AK 99775, USA; apbennett@alaska.edu

<sup>2</sup> International Arctic Research Center, University of Alaska Fairbanks, Fairbanks, AK 99775, USA; pbieniek@alaska.edu

\* Correspondence: valexeev@alaska.edu

**Abstract:** There is a growing need for proactive planning for natural hazards in a changing climate. Computational modeling of climate hazards provides an opportunity to inform planning, particularly in areas approaching ecosystem state changes, such as Interior Alaska, where future hazards are expected to differ significantly from historical events in frequency and severity. This paper considers improved modeling approaches from a physical process perspective and contextualizes the results within the complexities and limitations of hazard planning efforts and management concerns. Therefore, the aim is not only to improve the understanding of potential climate impacts on streamflow within this region but also to further explore the steps needed to evaluate local-scale hazards from global drivers and the potential challenges that may be present. This study used dynamically downscaled climate forcing data from ERA-Interim reanalysis datasets and projected climate scenarios from two General Circulation Models under a single Representative Concentration Pathway (RCP 8.5) to simulate an observational gage-calibrated WRF-Hydro model to assess shifts in streamflow and flooding potential in three Interior Alaska rivers over a historical period (2008–2017) and two future periods (2038–2047 and 2068–2077). Outputs were assessed for seasonality, streamflow, extreme events, and the comparison between existing flood control infrastructure in the region. The results indicate that streamflow in this region is likely to experience increases in seasonal length and baseflow, while the potential for extreme events and variable short-term streamflow behavior is likely to see greater uncertainty, based on the divergence between the models.

**Keywords:** climate change; extreme events; risk modeling; dynamical downscaling; natural hazards; climate adaptation



**Citation:** Bennett, A.P.; Alexeev, V.A.; Bieniek, P.A. Modeling of Future Streamflow Hazards in Interior Alaska River Systems and Implications for Applied Planning. *Water* **2024**, *16*, 1949. <https://doi.org/10.3390/w16141949>

Academic Editor: Adriana Bruggeman

Received: 23 May 2024

Revised: 2 July 2024

Accepted: 4 July 2024

Published: 10 July 2024



**Copyright:** © 2024 by the authors. Licensee MDPI, Basel, Switzerland. This article is an open access article distributed under the terms and conditions of the Creative Commons Attribution (CC BY) license (<https://creativecommons.org/licenses/by/4.0/>).

## 1. Introduction

There is a growing need for proactive approaches to planning for natural hazards in a changing climate. River systems in Interior Alaska are currently undergoing significant changes, which have the potential to amplify in a changing climate in the future. Warming temperatures, combined with increased precipitation, have been shown to increase permafrost thaw within the region [1,2] and could cause rapid subsurface warming and the decline of the region's near-surface permafrost [3,4]. Permafrost-rich environments experience a complex relationship with subsurface hydrology in this region, which represents a significant challenge for local communities in terms of mitigating hazards associated with the rapidly changing climate. Understanding how these systems are likely to be altered in the future is critical for river and ecosystem management, risk identification, and long-term planning for the built environment. There is a significant gap in our knowledge of how we connect observed and projected changes in the rapidly changing environment with rational mitigation efforts. On the technical and computational side, in areas lacking significant observational records, historical calibration is challenging; therefore, confidence in future

projected changes may reduce the ability to confidently engage in no-regret adaptation or mitigation measures.

Approaches to assessing peak streamflow, particularly in remote locations, may involve a wide range of methods including modeling, observed discharge measurements, and remote sensing [5–7]. Prior studies indicate that spring snowmelt streamflow in Interior Alaska rivers has declined in recent decades, particularly in snowmelt-dominated systems, although the minimum baseflow has increased in winter months [8–10]. Increased minimum baseflow has been closely linked with warming temperatures in the region, late-fall precipitation increases, and altered season lengths, leading to the deepening of the active layer and increased groundwater flow [11,12]. Studies also indicate that the region is expected to continue to experience increases in precipitation in the future [13], leading to greater uncertainty in the system with the future projected climate. Since most planning efforts are based on historical occurrences, significant ecosystem state changes can present unexpected challenges, including the amplification of existing hazards or the introduction of new hazards. The intent of this paper serves two primary purposes: (1) to enhance and improve model simulation approaches from a physical process perspective and (2) to contextualize modeling results within the complexities and limitations of hazard planning efforts. Based on this, the goal is to provide an important forward-looking perspective on predicting and understanding potential shifts in streamflow behavior and how these shifts need to be mitigated.

In this study, three Interior Alaska river systems were simulated using the WRF-Hydro modeling environment [14] to assess the potential future trajectories of mean and extreme streamflow using downscaled data from multiple climate models for a single future emissions scenario. These models were selected as part of a previous assessment of General Circulation Model (GCM) performance within Arctic Alaska and Canada [15]. As this work was primarily exploratory in nature, specific predictions were not made as to the outcomes. However, the expectations were that seasonality would continue to grow in the future, based on the aforementioned prior work in the region. Based on the results of these modeling efforts, the impacts were assessed in terms of policy and decision-making uncertainty and the limitations that may be associated with high uncertainty with regard to long-term climate adaptation measures. Therefore, in addition to improving the understanding of potential climate impacts on streamflow within this region, our second goal of this paper is not only to improve the understanding of potential climate impacts on streamflow within this region but also to characterize the steps needed to explore local scale hazards from global model outputs and the potential challenges associated with those steps.

## 2. Background

### 2.1. Study Area

Our study area was situated in Interior Alaska and included the Chena (5740 km<sup>2</sup>), Salcha (5350 km<sup>2</sup>), and Goodpaster (1770 km<sup>2</sup>) River basins (see Figure 1) [10,16]. These three basins flow into the Tanana River (66,205 km<sup>2</sup>) [10], a major tributary of the Yukon River system (853,300 km<sup>2</sup>), which eventually flows into the Yukon–Kuskokwim River Delta and exits into the Bering Sea [17]. All three basins are currently in areas with a high presence of discontinuous permafrost, where thawing has the potential to alter groundwater flow [17]. Local ecosystems consist primarily of subarctic boreal forests with coniferous-dominant vegetation [18], which are undergoing a shift toward a deciduous-dominated area, driven by warming temperatures and wildfire activity [19].

The climate is categorized as subarctic, with annual temperatures in the region ranging from very cold, dropping below  $-40^{\circ}\text{F}$  ( $-40^{\circ}\text{C}$ ) in wintertime, to very warm, often exceeding  $80^{\circ}\text{F}$  ( $26^{\circ}\text{C}$ ) in summertime [20]. Temperatures have trended up in the last few decades [21] and are expected to continue to rise in the future, with both minimum and maximum temperatures shifting upward [13]. Historically, precipitation in the region has typically been low, with annual means in low-lying areas below 300 mm in the Fairbanks area [17], while areas at higher elevations within the study area may exceed 700 mm of

accumulation annually [22]. The 2020 census indicates that approximately 100,000 people live in the study area, with the vast majority located in the Chena River basin downstream of and protected by the Chena Flood Control Project in and around Fairbanks and North Pole, Alaska (see Figure 1), with as many as 85,000 people at risk from a catastrophic failure of control measures [23,24].

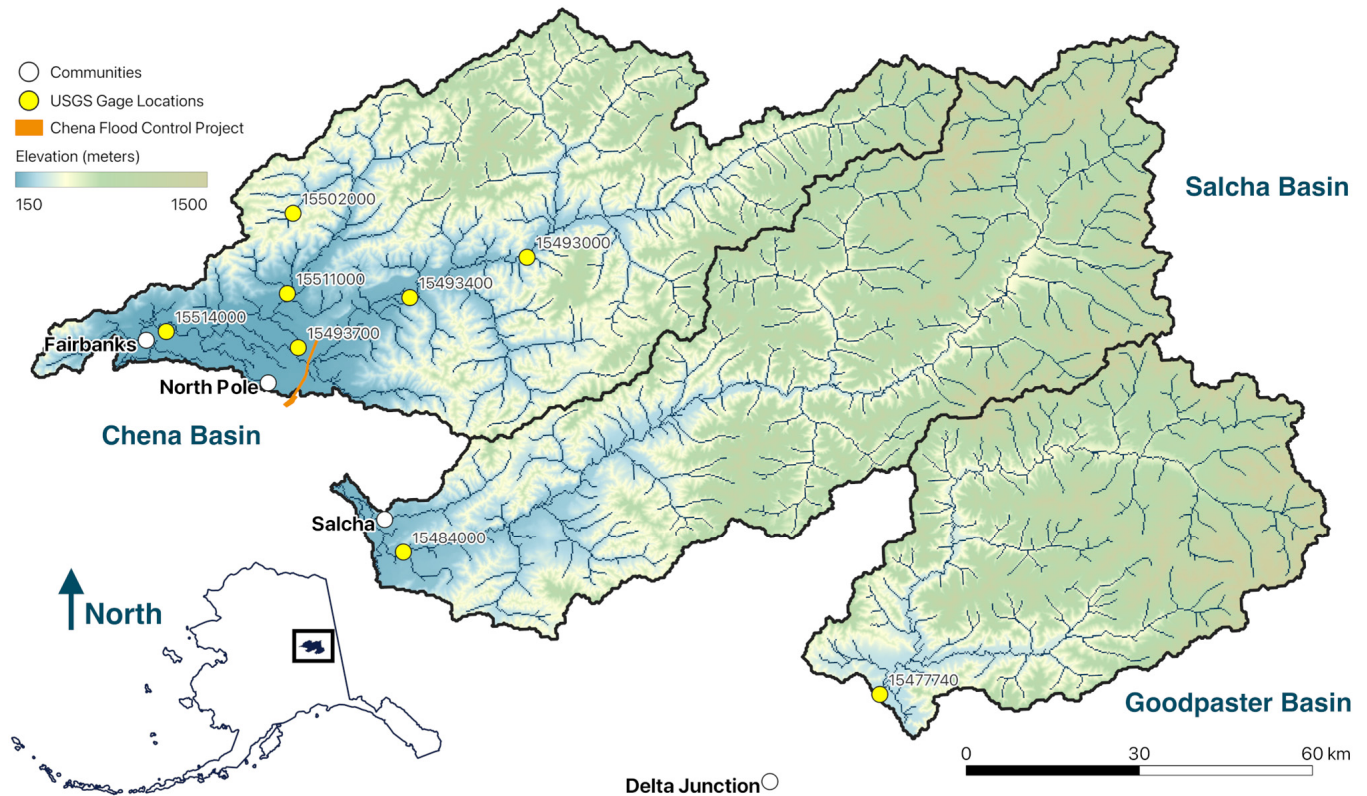


**Figure 1.** Map showing the three primary study areas. Chena (top left), Salcha (middle), and Goodpaster (bottom right) River basins. Gage locations are shown with yellow dots and their gage ID. Communities within the region are indicated by white dots. The orange line, near North Pole, Alaska, represents the extent of the Moose Creek Dam and Chena Flood Control project, including the reservoir and spillway into the Tanana River. The original Alaska IFSAR 5 m digital terrain model (DTM) is shown as a base layer in a green-to-blue gradient [25]. The inset map shows the state of Alaska, with the location of the study areas shown within a black rectangle.

## 2.2. Flood Control and Flood Events

The Chena and Salcha Rivers have significant influences on the nearby communities of Fairbanks, North Pole, and Salcha, Alaska. These river basins each have a history of generating flooding events throughout the region. Notably, the Fairbanks area was the location of an extreme flooding event in August of 1967, which resulted in USD 85 million in damages at the time [26], or over USD 775 million adjusted for inflation (calculated in August 2023) [27]. During the 1967 event, approximately 95 percent of the city of Fairbanks was flooded, with some areas being inundated with nearly 5 feet of water [26]. During the 1967 event, some streamflow gages in the region were completely destroyed, limiting the ability to collect data related to the flood [26]. This event prompted substantial changes to the management of local river flows, directly leading to the construction of the Chena Flood Control Project and the Moose Creek Dam, which was intended to divert water during high-flow events [28]. Shortly after the completion of the flood control project, increased instrumentation and monitoring efforts were established to assess the operational capabilities and impacts of the system on the local environment [29].

Since its installation in 1979 and first activation in 1981 [30], the Chena Flood Control Project has been activated 30 times (as of 2021) to prevent downstream flooding impacts [31]. The project is designed to manage peak streamflow such that downstream flow is limited to approximately 12,000 ft<sup>3</sup>/s (340 m<sup>3</sup>/s) through Fairbanks, based on its assessed channel capacity [32]. If the system reaches this capacity, the floodgates at the dam are lowered to divert excess flow into a connected reservoir. In an event where this reservoir capacity is exceeded, overflow is diverted into the Tanana River through a spillway past the Tanana Levee [24]. As of 2024, the flood control project is undergoing modifications and upgrades as part of a U.S. Army Corps of Engineers project to improve streamflow management and reinforce the embankment [33]. These upgrades are expected to be completed in 2026 [34]. This effort also reduces the potential for seepage under the main levee through the inclusion of deeper groundwater barriers [24,33]. Activation of the flood control system also impacts sediment accretion upstream of the dam and reduces nutrients downstream, which presents a series of challenges for flood diversion and wildlife within the area. While this flood control project primarily affects only one of the three study basins, it protects most of the population in the study area and therefore has a significant impact on human safety and the overall protection of the built environment of the region.

Flooding events in the Chena River basin typically fall under two primary patterns: spring snowmelt and intense summer rains [30]. Historically, the majority of these appear as summertime rain events, primarily occurring in June, July, and August, during short-duration, intense precipitation events [30,35]. The 1967 flood, for example, generated nearly 10 inches of precipitation within a 12-day period in August [26], approaching the total annual average for the area. The duration of the activation of the flood control project has varied substantially across events, with the longest event taking place in 1992 spanning 19 days and resulting in the only time excess flow poured into the Tanana via the spillway [36]. This event was unusual as it combined a heavy winter snowpack, late spring snowmelt, and intense rains.

Flooding events in this region can also be caused by ice-jams. Ice-jam occurrence is often a mix of hydro-meteorological conditions combined with stream morphology characteristics, such as sinuosity [37]. For instance, in 2020, the Chena Flood Control Project was activated due to a spring ice-jam event, which is seen as a semi-unique event in the history of the project, only having happened one other time, in 2002 [38]. However, in the Salcha River basin, the history of ice-jam flooding is more prevalent, with a number of events occurring in recent decades during spring breakup [39]. Streamflow rates in the Salcha River tend to peak at higher levels, despite having a similar overall extent as the Chena basin system (5740 km<sup>2</sup> for the Salcha basin versus 5350 km<sup>2</sup> for the Chena basin), potentially leading to more ice-jam effects [10]. During the 1967 floods, the Salcha River experienced intense flooding events, and while preventative removal of the gage at the time limited data gathering, manual measurements were later used to generate peak flow estimates of nearly 97,000 ft<sup>3</sup>/s (~2750 m<sup>3</sup>/s) [26]. Flooding in 2008 near Salcha was recorded as the most significant event since the 1967 event, with over 100 homes experiencing flooding [40]. Since 2012, as part of a railroad expansion project, an installed levee has helped to reduce risks associated with spring melt and river breakup events in Salcha [41,42].

While the Goodpaster River basin is significantly smaller than either the Chena or Salcha River basins, it has a higher proportion of its catchment area located above 600 m in elevation compared to the other study basins [16]. With no major settlements along the Goodpaster River, floods have a less direct impact on populations, but its inclusion offers an additional unmanaged river system for comparative analysis.

### 2.3. Streamflow Gages

Within the study area, the U.S. Geological Service (USGS) maintains multiple official streamflow gages, with six located in the Chena River basin, one in the Salcha River basin, and one in the Goodpaster River basin [43]. For consistency, the use of the USGS preferred

spelling of gage, rather than gauge, is used within this paper [44]. The placement of these gages and their record lengths played an important role in the calibration and analysis potential within this study.

The record length of most existing gages in the Chena River basin is limited when it comes to long-term historical as well as pre-dammed flow. The streamflow gage with the longest record is located downstream of the Chena Flood Control Project, near Fairbanks (15514000, Figure 1). However, since the completion of the flood control project in 1979 [30], the downstream record reflects a managed environment with the goal of preventing or minimizing flooding. Thus, any study of peak streamflow events must be compared to unmanaged areas along the river systems.

The nearest upriver gage to the flood control project, Chena River Below Hunts Creek (15493400) [45], was installed in 1989 and has operated nearly continuously since. Peak flow measurements from this gage align closely with peak flows from the upriver gage at Chena River near Two Rivers (15493000), with Kling-Gupta Efficiency (KGE) scores of 0.84, and it would be reasonable to assume within the same basin system that flow patterns downstream would similarly be reflected under a natural or unmanaged flow environment. The focus on the Chena River Below Hunts Creek gage (15493400) allowed for calibration as the furthest downstream point that is not under the active management of streamflow, providing closer comparisons to natural flow. Additional gages in the Salcha and Goodpaster River basins were used as secondary analysis sites, despite having a shorter observational record.

#### 2.4. Discontinuous and Sporadic Permafrost

Permafrost plays a significant role in ground hydrology, acting as both a barrier to downward infiltration, as well as a cause of the rapid degradation or alteration of previously existing groundwater and surface water patterns. Wildfires, warming, and heavy precipitation events can modify permafrost extent and features, resulting in changes to subsurface flow dynamics that may generate permanent changes to existing streamflow patterns and local ecosystems [46]. In some cases, permafrost degradation can occur rapidly, through short-term extreme events [47]. In Interior Alaska, there is a significant presence of sporadic and discontinuous permafrost [48], which presents additional interactions for streamflow due to its susceptibility to rapid thaw events, altering subsurface hydrology [1]. Warming temperatures, combined with greater snow cover, have already been attributed to increases in active layer thickness in the region and increases in permafrost temperatures in the last few decades [49]. Most recently, between 2017 and 2019, there have been numerous examples of sites within the region where the permafrost has not completely refrozen in winter, generating suprapermafrost taliks, or patches of ground that are unfrozen but sit above the permafrost and below the active layer [49]. In the future, permafrost thaw models indicate a substantial decline in sporadic and discontinuous permafrost within Interior Alaska, which is likely to impact seasonal runoff patterns, as soil storage capabilities and ground connectivity increase due to a reduction in ground ice [4].

#### 2.5. Hazard Assessment

As with many regions, the rivers of Interior Alaska are an important part of the natural ecosystem and play an integral role in the built environment of populations living within proximity to riverine ecosystems. This role is deeply connected to flooding events, which act as potential hazards to the population, and infrastructure (e.g., roads, airports, houses). Traditionally, flood hazards have often been assessed based on a recurrence interval (e.g., 1 in 100 years, 1 in 10 years, etc.), sometimes referred to as a return period. These intervals are normally derived from known historical occurrences and sometimes an extrapolated probability distribution based on those occurrences and may be represented as something like  $T_r = 1/P$ , where  $T_r$  represents a return period and  $P$  represents the annual exceedance probability at a certain threshold [50]. Inverting this approach offers an annual exceedance probability (AEP), which provides the percent chance of the event occurring annually

(e.g., 1 percent per year, 10 percent per year, etc.) [51]. The 1 percent AEP has been used by the United States National Flood Insurance Program since the 1960s as the basis for the insurance program [52]. These thresholds help to determine insurance rates for those living within flood-prone areas but may lack nuance when it comes to the variability of specific events, which vary in intensity, duration, and frequency and may have high spatial variability [53].

The approach to defining flood hazards focuses on an assumption of stationarity in flood recurrence causes. However, it is increasingly being recognized that the non-stationarity of flood recurrence and other hazards may make it difficult to use this approach in the future as system state changes lead to entirely new hazard regimes [54]. In areas where climate change is expected to produce events that significantly depart from known event probabilities, it becomes important to consider extreme events under a range of possible future conditions to better understand the ability of existing systems to withstand those extremes. Emerging extreme events, which may not have been experienced in the past within a given region, present additional challenges for local planners and residents, as this introduces new uncertainties and may require significant study to proactively mitigate associated hazards [55]. However, perceptions of risk are often counterintuitive, as indicated by recent surveys highlighting that those living in high-flood-risk areas may hold lower levels of risk perception surrounding those events [56]. Perception of risk is also often influenced by multiple factors, with awareness of risk being only one of many components, while preparedness against a particular risk and levels of worry or stress about those particular risks also influence their prioritization [57].

### 3. Methods

The WRF-Hydro model, which offers an open-source, flexible, and extensible modeling architecture, was selected as the primary modeling tool for simulating streamflow in this study [58,59]. WRF-Hydro includes a land-surface module, overland routing, and channel routing and can be coupled directly with WRF atmospheric models or run in standalone mode, which was the approach used in this study. WRF-Hydro was selected due to its basis as part of the National Water Model [60] and to act as a testbed for Interior Alaska basins. While WRF-Hydro has seen limited applications in Alaska, it was adapted for the region during the study period and is now in limited operational use in some regions of the state [61]. While WRF-Hydro has been widely tested in the contiguous 48 states, differences in Alaskan ecosystems, including subsurface dynamics, seasonal cycles, and local infrastructure, required modifications to the study region. WRF-Hydro has a very detailed soil scheme, explicitly solving Richard's equation for the propagation of moisture, with hydraulic conductivity being a function of soil properties (e.g., soil can be rocky with a lot of voids or very dense and uniform in the case of clay) and temperature (hydraulic conductivity values are significantly reduced when soil is frozen), which makes it suitable for cold environments.

Substantial experimentation, both in the initialization and setup of the model, was required to correctly account for permafrost through frozen ground modules. Additional effort was also required to identify and develop datasets that would correctly represent regional hydrologic behavior, particularly in areas with active flood control structures, due to their influence on rerouting streamflow. Input datasets required to run the WRF-Hydro model included topography and climate-forcing data.

The WRF model was used to dynamically downscale the climate data used to force and calibrate WRF-Hydro, following similar prior work at 20 km [62], taking reanalysis and GCM data from coarse scales to produce high-resolution (1 km) air temperature at 2 m, precipitation, specific humidity, wind, radiative forcing, and surface pressure, at hourly time steps. To adjust for the overrepresentation of precipitation in the dynamically downscaled WRF model outputs, future climate forcings were then bias-corrected at hourly time steps using Quantile Delta Mapping (QDM) approaches, which allows for the preservation of relative changes [63]. The calibration of the model focused on a comparison of the

European Centre for Medium-Range Weather Forecasts (ECMWF) ERA-Interim data to key streamflow gage locations and overlapping periods between reanalysis and projected data [64]. Analysis of WRF-Hydro model output data was performed using Python-based geospatial and analysis libraries, leveraging matplotlib [65], numpy [66], pandas [67], and xarray [68] to summarize and visualize model outputs.

### 3.1. Model Setup

WRF-Hydro simulations were developed using version 5.1.1 of the model [14]. Simulations were run using Weather Research and Forecasting (WRF) [69], downscaled data for the ERA-Interim reanalysis dataset [64], and two climate models selected from the Intergovernmental Panel for Climate Change (IPCC) Coupled Model Intercomparison Project (CMIP) phase 5 [70], including the Community Climate System Model (CCSM) version 4 from the National Center for Atmospheric Research (NCAR) [71] and Climate Model version 3 (CM3) from the Geophysical Fluid Dynamics Laboratory (GFDL) [72]. Both models were run using their outputs from Representative Concentration Pathway (RCP) 8.5 [73]. These two models were selected based on prior work showing CCSM and GFDL ranked first and third, respectively, among 21 CMIP5 GCMs in the simulation of the seasonal cycles of temperature, precipitation, and sea level pressure over Alaska [15]. RCP8.5 was selected as the highest forcing scenario with the greatest degree of warming in Alaska over lower scenarios such as RCP4.5 [74] and because observed carbon dioxide emissions have continued to best track RCP8.5 [75]. Both CCSM and GFDL were run for three time periods (2008–2017, 2038–2047, and 2068–2077), while ERA-Interim was run for 2001–2018, including the overlap period between the two GCMs. Each run used the parameterized landscape setup from the output of the calibration results as the starting point, described later in this section, offering direct comparisons in time spans between reanalysis and modeled datasets. Simulations were performed using overland flow and gridded diffusive wave routing, at an hourly time step, for the entire simulation period, for each of the six periods plus the historical periods. As discussed regarding the domain setup, model resolution for the reach characteristics was set at 250 m, while WRF forcing data were at a resolution of 1 km.

### 3.2. Domain Setup

As portions of the study domain represent managed waterways, it was necessary to develop a domain that properly reflected flood control structures in the area (levees, dams, etc.) that may alter the flow of water differently than a natural flow regime. Thus, we adjusted the flow and routing layers using the WRF-Hydro preprocessing tools [76]. Early efforts, using default digital elevation model (DEM) layers, led to overflow between the two basin systems. This occurred primarily due to coarse DEMs (90 m) failing to effectively capture the widths of those flood control structures, resulting in unexpected overflow events between basins. This result also offered an unexpected highlight of the importance of the existing control structures, and the potential for spillover should those systems fail and natural flow be restored.

Routing paths and basin extents were generated programmatically using the WRF-Hydro pre-processing tools for the National Center for Atmospheric Research (NCAR) [76], with the Alaska IFSAR dataset using the digital terrain model (DTM) acting as the primary DEM layer for the domain, which covered the entire study domain at a 5 m resolution [25]. The DTM was chosen to best represent the direct flow surface for routing, which largely excluded the heights of vegetation, which could inadvertently affect routing. IFSAR was then upscaled to 250 m for computational efficiency during simulations. Different minimum basin stream size values were tested, and a final value of 100 cells was used in the routing to identify streams to strike a balance between accuracy and computational efficiency.

The total area of the domain was established to include three main basin systems: the Chena, Goodpaster, and Salcha (see Figure 1). The primary comparative locations for forecast points were identified as USGS gage 15493400 (Chena, below Hunts Creek),

15484000 (Salcha, near Salchaket), and 15477740 (Goodpaster, near Big Delta). These locations represent gaged locations for each basin that are not subject to flow restrictions from flood control measures, allowing for an analysis of natural flow regimes. Lakes and reservoirs were not included as part of this work, as the primary emphasis was on extreme events and scouring that occurs during high flow. However, the resolution of the DTM can support these efforts in the future.

For each actively maintained USGS gage location, however, a forecast point was identified within the routing in order to provide analyses and comparisons. In addition to observation sites, an extra forecast point was added to each basin to gather the total outflow from each of the basins. Manual correction of gage locations was applied in cases where gages were not perfectly aligned with identified reach segments within the model to align forecast points with the nearest available gage reach segment.

### 3.3. Forcing Data

The forcing data in this set of simulations were produced as part of a larger project focused on the modeling of Interior Alaska river systems in order to identify implications for ecosystem management and impacts on fish populations within the study domain [77]. As high-resolution forcing data for the study area were previously unavailable, the development of these datasets was necessary. Historical and future forcing data were developed through dynamical downscaling within WRF of the ERA-Interim historical reanalysis dataset and projected climate data for RCP 8.5 of the GFDL and CCSM models.

The dynamical downscaling approach applied in this study was based on work previously performed for statewide Alaska downscaling efforts [62], and existing tools and expertise were leveraged to produce a 1 km resolution product centered on the study region, based on the bounding box visible in Figure 1. The new 1 km downscaling product followed much of the WRF physics options outlined in Bieniek et al. [62], which consisted of the RRTM radiation scheme, Mellor–Yamada–Janjic planetary boundary layer scheme, Monin–Obukhov surface layer scheme, and Noah land surface model. A key difference was that there was no cumulus scheme used as the 1 km spatial resolution was convective permitting, and the Goddard cloud microphysics scheme was employed after visually comparing the precipitation outputs with historical radar observations for a summer test period. Testing using a nested domain revealed that the primary impact on the downscaled outputs was primarily on the spatial distribution of summer precipitation, with minimal differences in the winter. For this study, a single 1 km resolution domain was used to limit the computational requirements of the downscaling.

The downscaled WRF runs were conducted for 54 h periods, which included a 6 h spin-up that was discarded, producing successive 2-day runs spanning each simulation period. Snow depth from the end of each prior 2-day simulation was used to initialize the next simulation period to provide a temporally consistent, high-resolution snowpack. Post-downscaling, WRF outputs were adjusted to align with the WRF-Hydro model input requirements, such that the hourly accumulation of precipitation was converted to precipitation rates in mm/s.

### 3.4. Bias-Correction

Initially, uncorrected simulation runs of the future projected models (CCSM and GFDL) had significant precipitation biases, which resulted in a high number of extreme events over the observed period. These issues appeared to originate within the dynamically downscaled outputs, inherited from the GCMs and ERA-Interim data, indicating that all of these datasets produced higher rates of precipitation in the region, although to varying degrees, when compared to PRISM precipitation baseline data [78], as seen in Figure 2. This uncorrected set of model runs produced both historical and future simulations that far exceeded historical flow rates, making it challenging to properly assess change over time. However, analyses of the high precipitation bias in these models aligned with previous work assessing coarser downscaling efforts in the region, indicating that both CCSM and

GFDL projections appear to produce wetter than expected conditions over the observed period within the study region [62]. Based on this early evaluation, it was determined that bias-correction approaches would be necessary to accurately represent precipitation for the study region and be able to identify decadal shifts more clearly.

### 2008–2017 Seasonal Average Precipitation (mm)

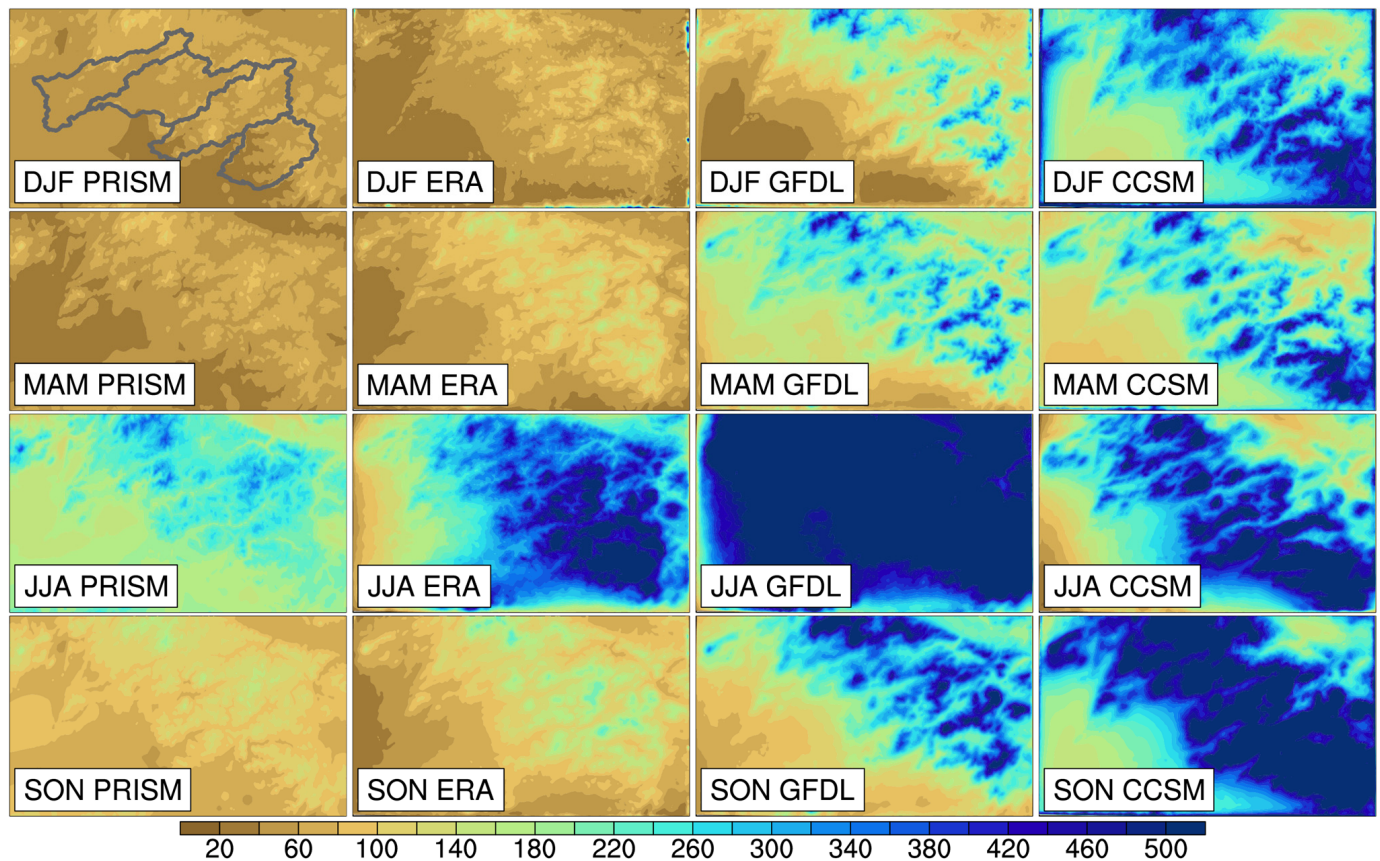


**Figure 2.** Multi-model precipitation comparison. Three-month groupings of seasonal precipitation over the study area, with PRISM as the baseline, showing dynamically downscaled ERA-Interim and RCP 8.5 for GFDL and CCSM.

For the needs of this study, the xclim package, which provides numerous built-in bias-correction and indicator tools, was used to bias-correct the downscaled datasets for GCMs, both for historical and future time periods [79]. QDM was selected as the training and adjustment method for bias-correction in order to better preserve extreme events within future datasets as it has been shown to increase the ability to represent and maintain peak flow events and has shown greater preservation of relative changes, particularly when correcting precipitation [63].

Precipitation data were bias-corrected through multiplicative scaling to retain the intermittent nature of precipitation in the region, while temperature data were corrected via an additive application of deltas. Data were corrected using a monthly grouping, with 2008–2017 ERA-Interim data used for the reference dataset and the 2008–2017 period used as the historical period for each GCM. Biases were calculated using the full month and then applied to temperature and precipitation within the modeled time periods (2008–2017, 2038–2047, and 2068–2077). Attempts were made to use larger quantile sets (50 instead of the default 20), but this resulted in amplified extremes within the observed overlap period and was discontinued.

Comparisons between pre- and post-bias-corrected datasets were assessed during the overlap period to evaluate GCM improvements against ERA-Interim baseline data. Bias-corrected temperatures followed similar annual and seasonal patterns for both CCSM and GFDL. Precipitation data varied more significantly between models and decades, with annual variability remaining higher in CCSM in future decades, while GFDL presented a more general upward progression of precipitation as the decades advanced (see Figure 3). CCSM produced seasonal behavior including steeper monthly average precipitation increases, but the total annual precipitation rose to higher maximums in GFDL, exceeding 700 mm annually (Figure 3).

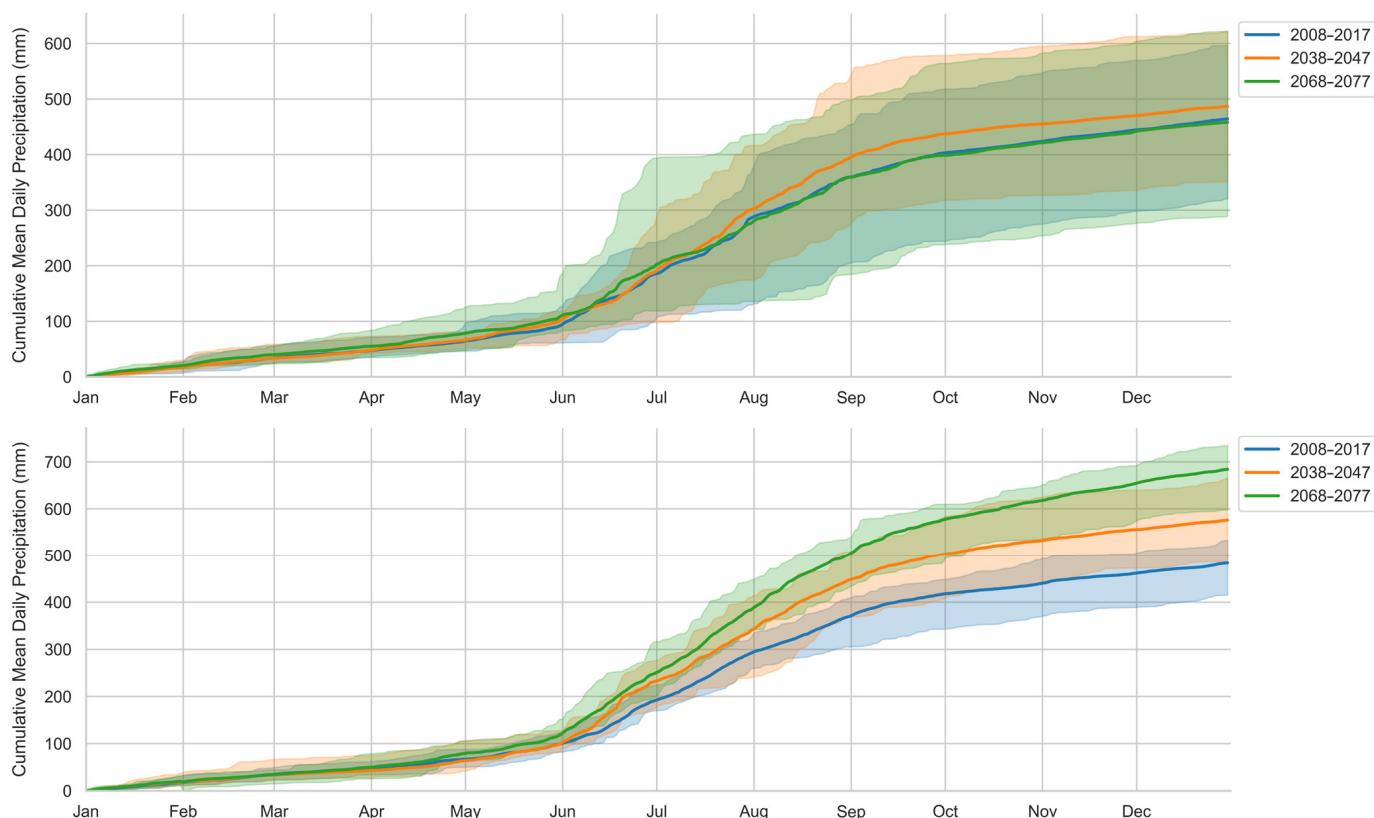


**Figure 3.** Model precipitation. Bias-corrected mean cumulative annual precipitation data for the full domain, CCSM (**top**), and GFDL (**bottom**). Bands represent annual minimums and maximums for each time period.

### 3.5. Calibration

The WRF-Hydro model was calibrated using PyWrfHydroCalib [80], an internal parameter sensitivity and analysis package written in Python and R, developed and maintained by NCAR. This package makes use of the R package hydroGOF (to perform goodness-of-fit testing) behind a series of controller scripts to streamline the calibration process across basins and manage spin-up, calibration, and validation phases [81]. This allowed for a semi-autonomous, minimally supervised, and time-reduced calibration of WRF-Hydro domains and streamflow, based on selected metrics, and was designed to allow for a high number of subdomains to be calibrated across major basins. This toolset was originally developed to assist NCAR in the calibration of basins throughout the contiguous United States as part of the National Water Model [60] and has been tested across thousands of basins in the contiguous United States.

For this study, as replicating peak flow events was the primary goal, KGE was selected as the best available calibration within selected toolsets as it has been shown to have improved effectiveness at replicating peak flow events while reducing the loss of other parameters' performance [82]. While scores above certain thresholds may be considered

good for KGE, this depends on the aim of the modeling efforts [83]. In this case, since semi-automated fit testing was performed, scores were used to inform points of diminishing returns, not as a specific threshold for success. WRF-Hydro was calibrated in two distinct batches, based on available computational resources, with the first beginning with default initial conditions for 250 iterations and the second of over 225 iterations using improved starting conditions. The spin-up phase, especially in cold environments, is particularly challenging, as there is no simple method to initialize it in a climatologically consistent way, especially over complex terrain. Assigning negative temperatures in a uniform way to soil layers does not solve the spin-up challenge because soil temperatures have very pronounced seasonal dependence and variability, based on soil properties, vegetation, terrain, and other factors at each grid point. Therefore the spin-up was chosen to be long enough (2001–2010) to establish baseline soil parameters and frozen ground, while the calibration phase was focused on 2013–2015, both to account for high flow events that occurred during that period and to balance computational efficiency [35]. The validation phase was then set for 2016–2018 to test calibration performance for each iteration.

The first round of calibration produced a maximum KGE score of 0.71, while the average of all runs was 0.60. The highest performing set of parameters produced were then used as starting conditions for a second batch and produced a maximum KGE score of 0.728, with an average KGE across all runs of 0.61. The final highest-performing run was used to establish the baseline for climate simulations and future projection-based runs. The negligible improvements of the second batch of runs indicated diminishing returns that did not justify further rounds. The calibrated model was re-run through an extended reanalysis period within the ERA-Interim-based forcing data to provide comparisons for 2001–2018. Additional details about the calibration, sensitivity and variability, and selection of the highest-performing parameterization can be found in the Supplementary Materials, in Figures S1–S15.

## 4. Results

### 4.1. Calibration Results

Using the derived model calibration parameters produced simulated maximum streamflow values comparable with observed streamflow peaks for the Chena River but led to poorer performance for the Salcha River, where maximums exceeded observed events (Figures 4 and 5). Both seasonal streamflow distributions and peak flows for the Salcha River indicated more substantial mismatches between observed and modeled data, despite being one basin adjacent to the Chena River, where calibration was primarily focused. For the Salcha, streamflow was simulated with improved skill for two years (2007 and 2012), even though these were not part of the calibration years. However, the overall performance was still degraded when compared to the Chena. This may be improved upon in future studies through the refinement of components such as subsurface soil properties, frozen ground conditions, and vegetation layers and, most importantly, by basin-specific calibration. Comparisons between the observed and simulated data can be seen in Figures 4 and 5. Wet bias in the model forcing data (as seen in Figure 2) was present in the WRF downscaled ERA-Interim data and GCM outputs when compared to PRISM. While attempts were made to avoid overfitting during calibration, this bias persisted in the projections as well since calibration was based on the ERA-Interim reanalysis data, rather than being corrected to PRISM.

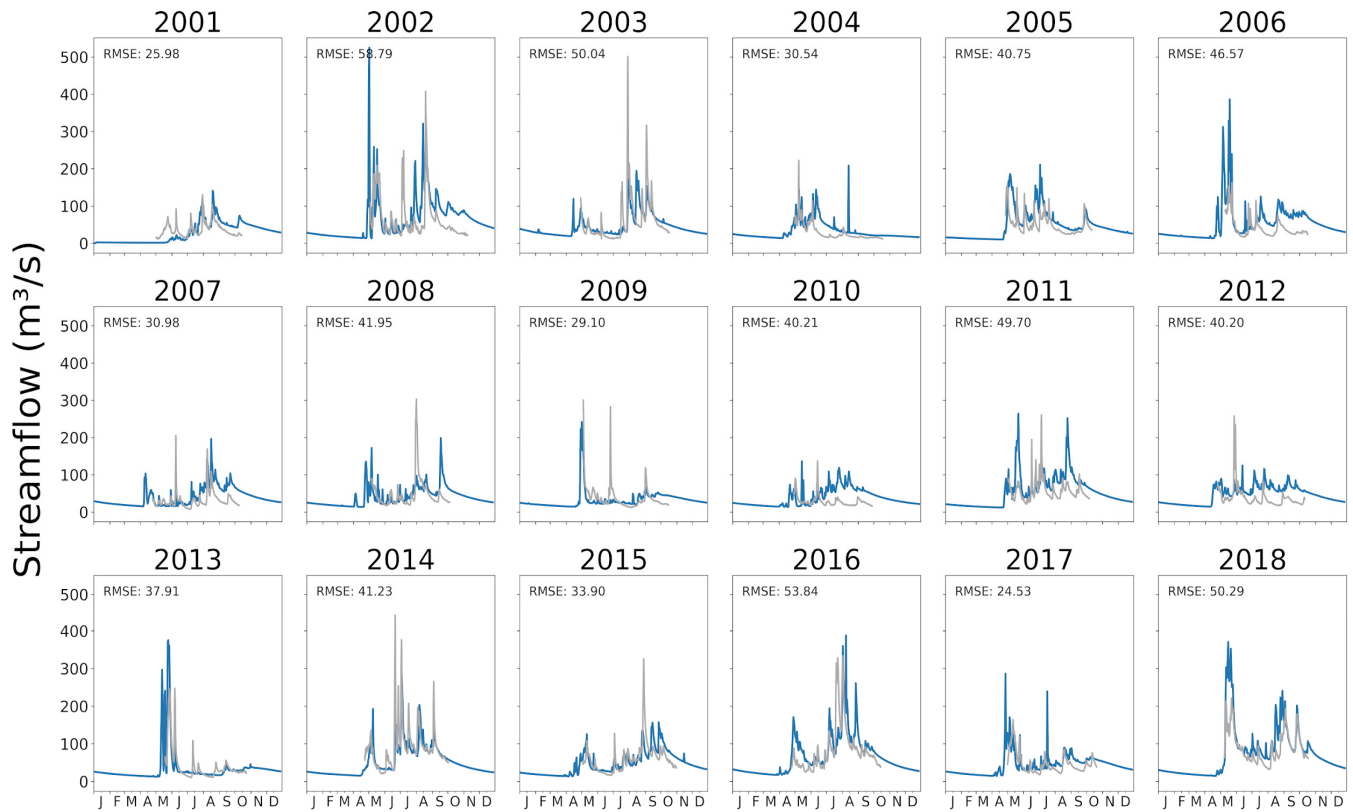


**Figure 4.** Comparison of observed gage data (gray) at Gage ID 15493400 (Chena below Hunts Creek) with simulated model runs (blue) for the 2001–2018 period, Jan–Dec, following calibration.

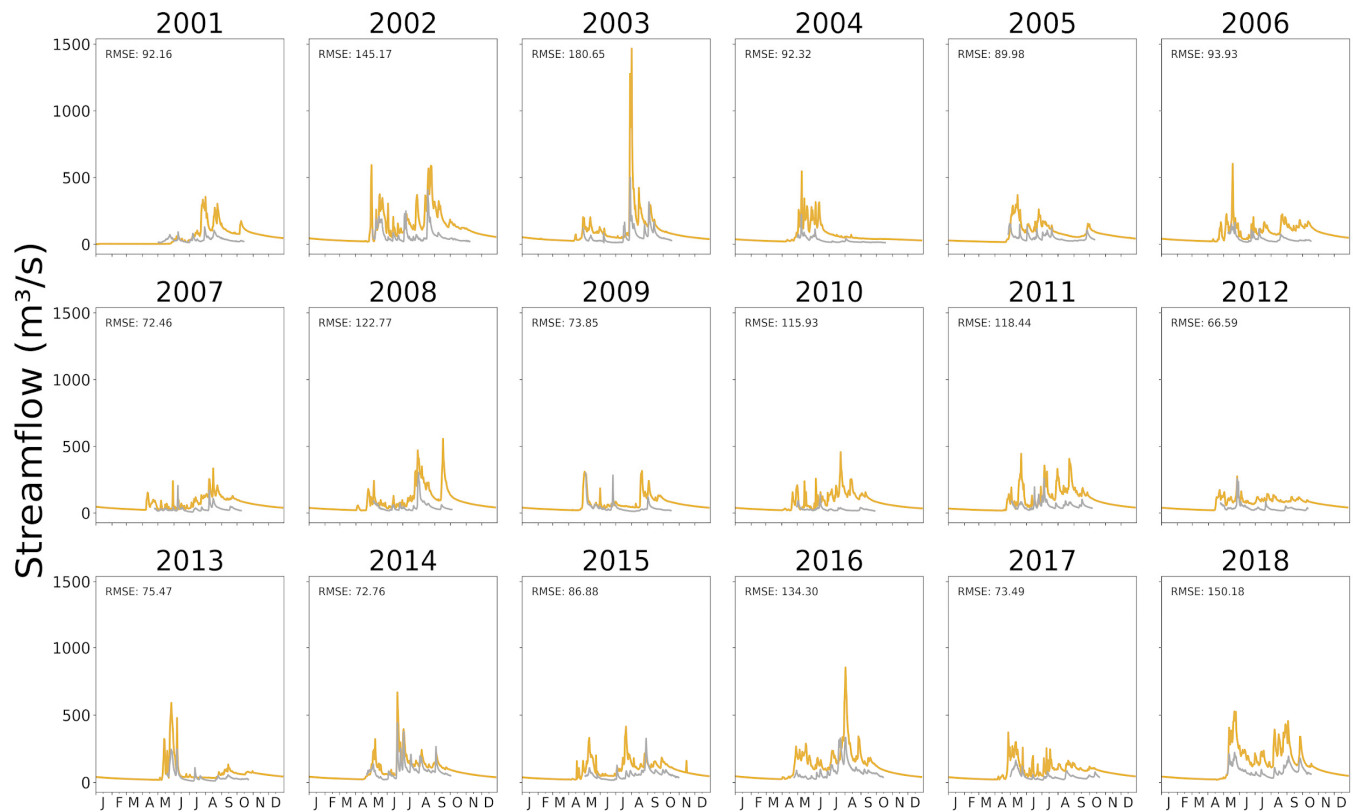


**Figure 5.** Comparison of observed gage data (gray) at Gage ID 15484000 (Salcha) with simulated model runs (gold) for the 2001–2018 period, Jan–Dec, following calibration.

#### 4.2. Model Divergence

The divergence between future GCM-driven simulations presented itself in the distribution of both extreme events and non-extreme streamflow. This divergence can be seen in Figures 6–8, representing all three basins within this study. For these plots, the box represents the interquartile range of annual means or maximums, while whiskers represent the highs and lows within the variance from the quartiles. Outliers are marked with circles. GFDL showed a clear increase in mean annual streamflow and total streamflow when compared to both the historical period and the CCSM simulations, as well as a more modest increase in extreme flow events (see Figure 6). Variability tended to be significantly lower within GFDL as opposed to CCSM, and simulations produced consistently higher streamflow across basins, in some cases producing a near-two-fold increase in streamflow over the duration of the simulated years, particularly in mean annual flow. This was consistent with the precipitation patterns identified earlier, with GFDL experiencing consistent decadal increases in annual precipitation. While GFDL generally maintained a narrower range of variability in most decades and basins, the 2038–2047 and 2068–2077 periods for the Goodpaster River basin produced particularly high variability in maximum flows, which narrowed some by the 2068–2077 period (Figure 8).

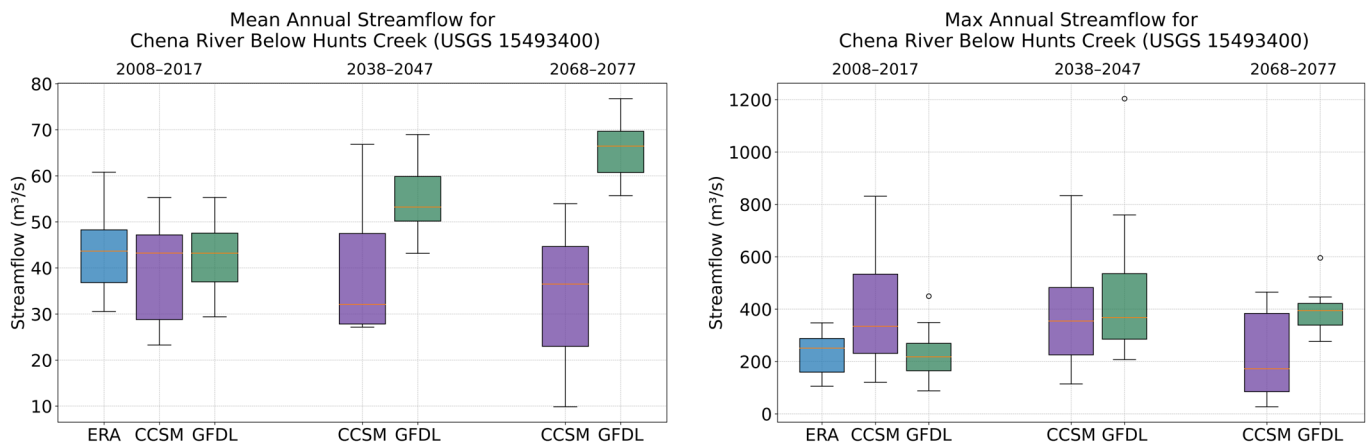


**Figure 6.** Mean and max flow for Chena River basin. Annual mean flow (left) and maximum flow (right) for USGS Gage ID 15493400 (Chena River, below Hunts Creek) for the observed period (blue) and projected CCSM (purple) and GFDL (green) simulations.

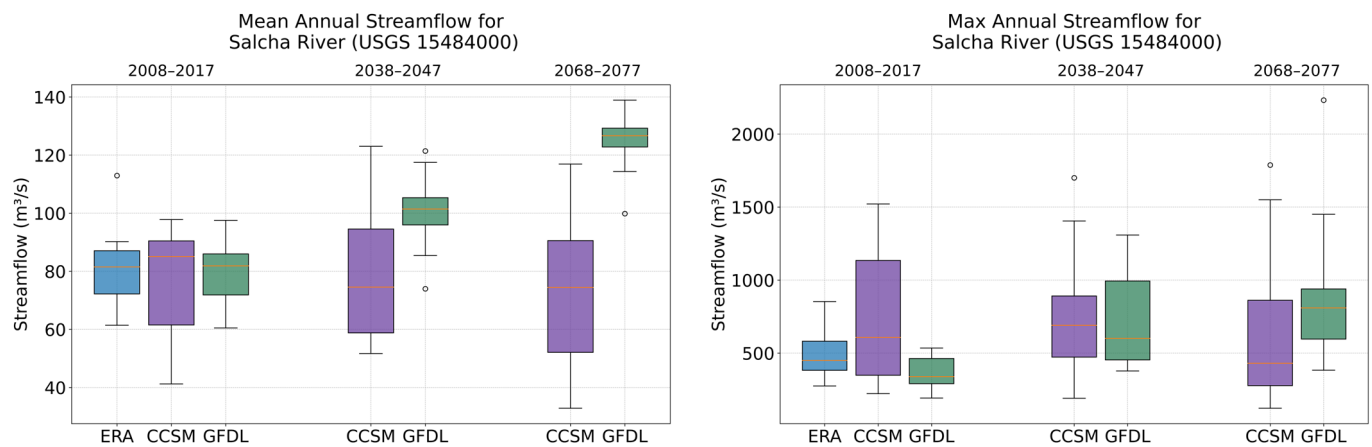


**Figure 7.** Mean and max flow for Salcha River basin. Annual mean flow (left) and maximum flow (right) for USGS Gage ID 15484000 (Salcha River) for the observed period (blue) and projected CCSM (purple) and GFDL (green) simulations.

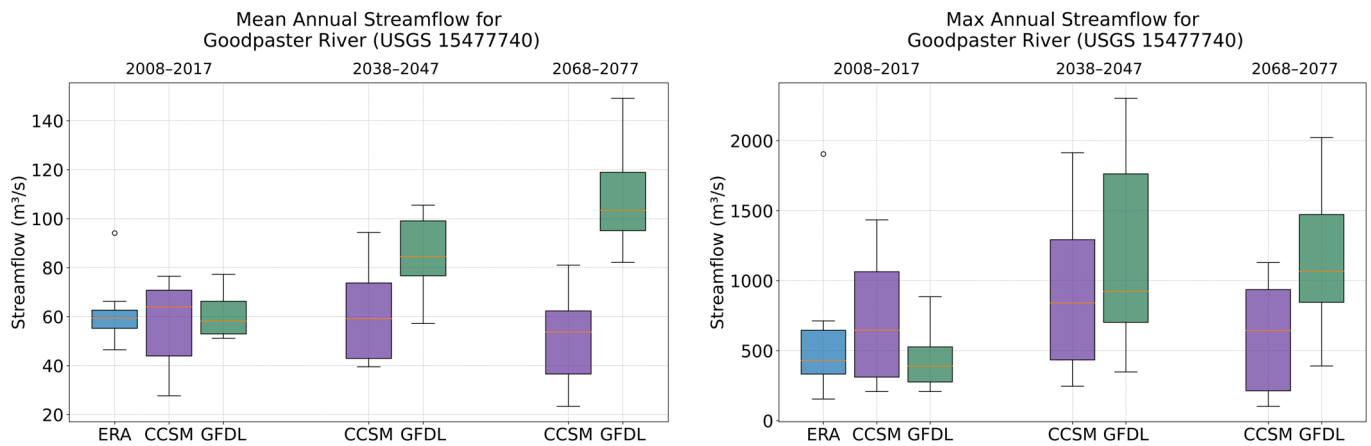


**Figure 8.** Mean and max flow for Goodpaster River basin. Annual mean flow (**left**) and maximum flow (**right**) for USGS Gage ID 15477740 (Goodpaster River) for the observed period (blue) and projected CCSM (purple) and GFDL (green) model runs.

CCSM presented a modest but subtle downward trend in long-term streamflow relative to the historical period, indicating declines in mean annual streamflow and widening variability in annual maximums when compared to historical values (Figures 6–8). This pattern was presented similarly across the basins, with CCSM experiencing higher variability in maximum streamflow events compared to both GFDL and ERA simulations, particularly during the observed period (2008–2017), when extreme streamflow events in CCSM nearly doubled compared to those generated by ERA-Interim simulations across all basins (Figure 7). Therefore, it was important to assess both GFDL and CCSM streamflow in relative terms as well when compared to their own historical periods. In future decades, a relative decline in maximum streamflow was observed, while GFDL experienced outliers (e.g., extremes) late into the 21st century.

#### 4.3. Seasonality

Based on temperature trends in the region, and the previously mentioned expectations of multi-seasonal warming, the results indicated a lengthening of the streamflow season, with earlier snowmelt events and higher flow events extending later into the warm season. These seasonal expansions can be seen in Figure 9, showing snowmelt-driven streamflow events occurring one month earlier, in April instead of May, and elevated flow persisting into late fall. Rainfall-driven events during late summer experienced an increase in magnitude over earlier decades. In the case of GFDL, the result was a more bi-modal pattern of streamflow increase, with both spring and late-summer high-flow patterns. CCSM, however, experienced a significant increase in mid-summer streamflow, particularly in the 2038–2047 period, driven by multiple years of high precipitation (as seen in Figure 3).

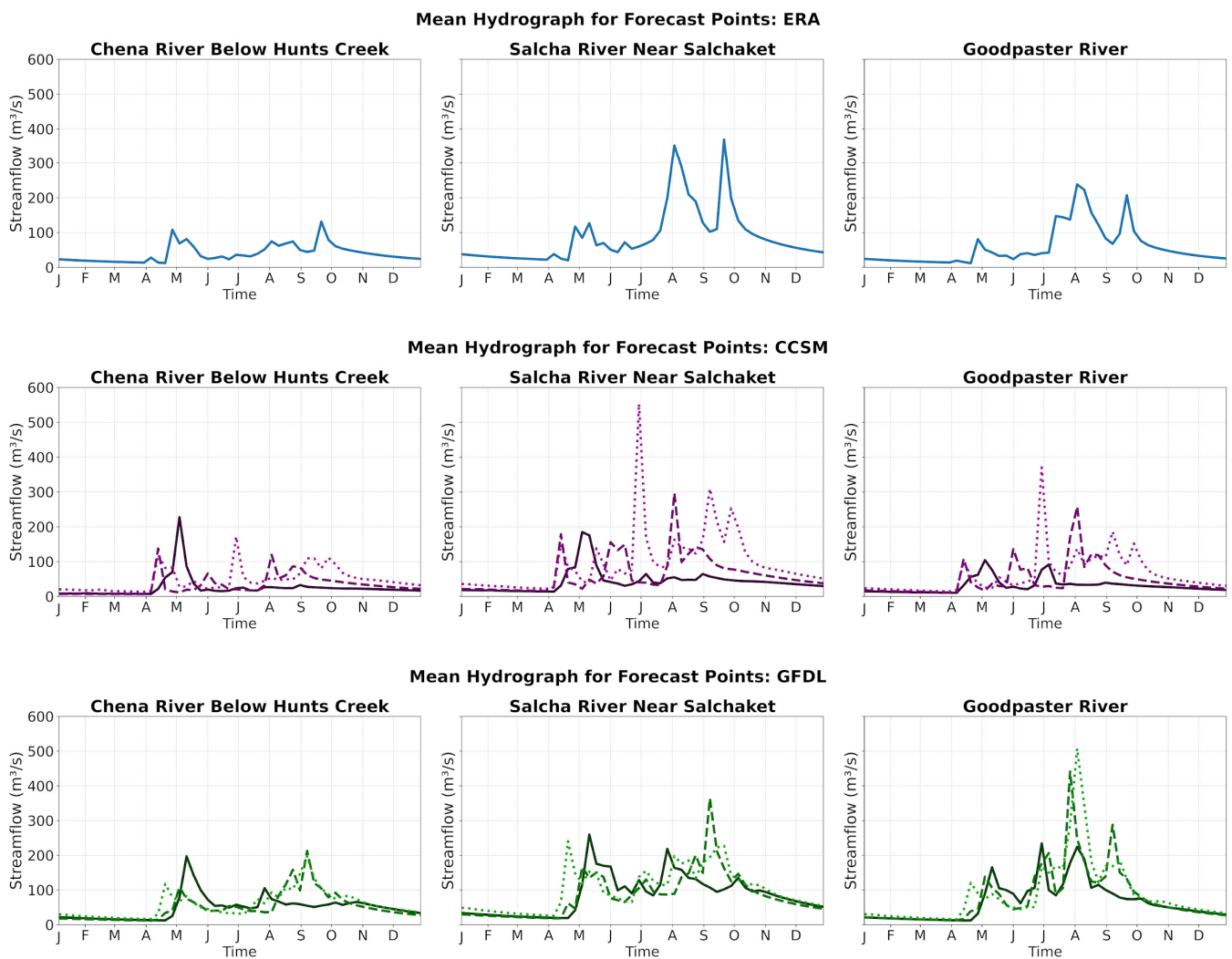


**Figure 9.** Mean weekly streamflow averaged by decade. Mean weekly streamflow hydrograph by decade comparison for CCSM (top, purple shades) and GFDL (bottom, green shades) during the 2008–2017 (dark solid line), 2038–2047 (medium dashed line), and 2068–2077 (light dotted line) time frames for the Chena River below Hunts Creek, Salcha River near Salchaket, and Goodpaster River gage locations.

#### 4.4. Flood Control Implications

Based on the previously estimated  $12,000 \text{ ft}^3/\text{s}$  ( $340 \text{ m}^3/\text{s}$ ) threshold used to restrict downstream flow rates, the frequency of activations of the flood control project in the future increased significantly under GFDL (see Figure 10), with over three times as many events in the mid-decade period and over eight times as many events in the later decade, while flood frequency appeared to stay within a similar range under CCSM in the 2038–2047 period followed by a decline (see Figure 11). GFDL indicated a consistent increase in both the duration and frequency of flood events. Particularly under GFDL, these results indicate that flood control management may be required more frequently in the future, with an increased number and longer activations of the floodgates, assuming no changes in current flood control infrastructure occur. Previous activations of the Moose Creek Dam have highlighted the potential for nearby residences and areas to experience groundwater infiltration, as the dam is unlined and subject to hydrostatic pressure transfer. Newer renovation projects may help to reduce, but not eliminate, these challenges, and may be tested under the extremes indicated for GFDL [24].

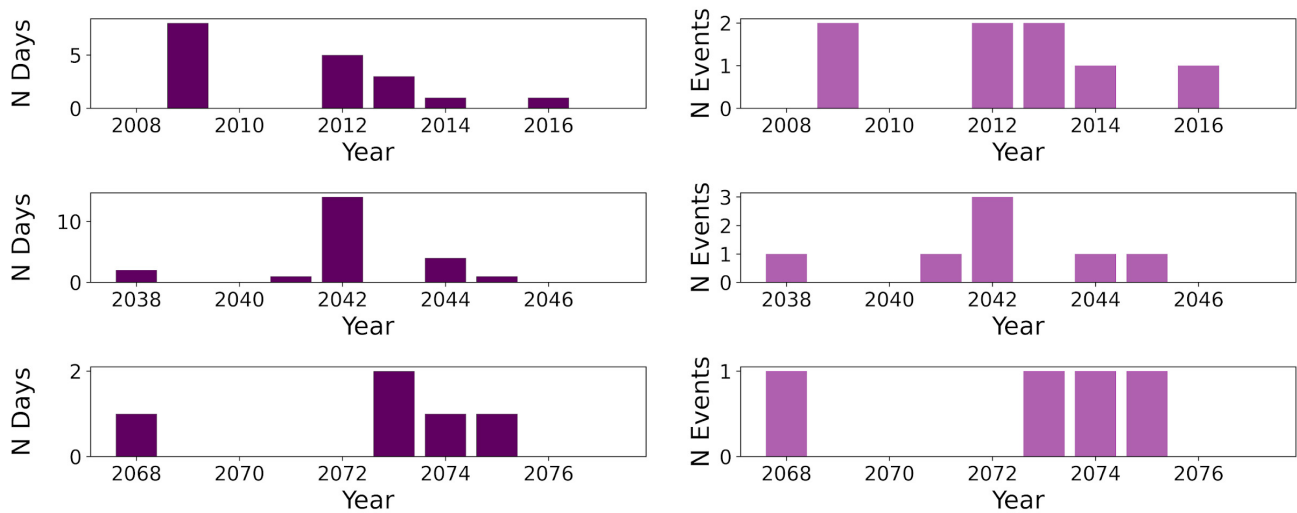


**Figure 10.** Flooding events for CCSM. Events modeled under CCSM indicating the crossing of pre-established flood control thresholds. Dark purple represents the number of days where streamflow rates exceeded the 12,000 ft<sup>3</sup>/s (340 m<sup>3</sup>/s) threshold. Light purple represents the total number of events per year exceeding that rate. Each event represents one or more days where the streamflow continuously exceeded thresholds.

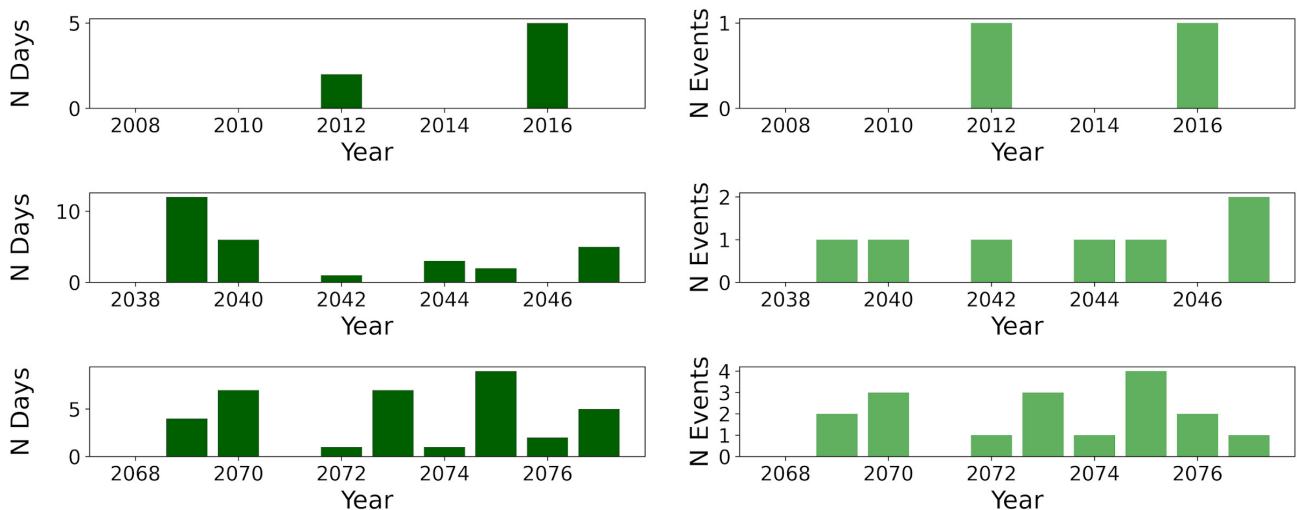


**Figure 11.** Flooding events for GFDL model. Events modeled under GFDL indicating the crossing of pre-established flood control thresholds. Dark green represents the number of days where streamflow rates exceeded the 12,000 ft<sup>3</sup>/s (340 m<sup>3</sup>/s) threshold. Light green represents the total number of events per year exceeding that rate. Each event represents one or more days where the streamflow continuously exceeded thresholds.

**5. Discussion**

This study highlights a number of important factors when it comes to the behavior of future streamflow within the study area, emphasizing the potential for future projections to improve our understanding of Arctic riverine systems in terms of shifts in seasonality, the intensity of extreme events, and changes to mean annual streamflow within river systems. Shifts in infrastructure demands and the need for mitigating controls are also important factors that present opportunities for decision-makers to plan around system changes well in advance of those changes being realized. This study helps to advance this effort by offering a future perspective on shifts to streamflow within the region, while prior work was primarily focused on historical changes. This can allow for a potential reduction of impacts through proactive adaptation, whether through nature-based solutions (e.g., the

establishment of non-buildable floodable lands) [84] or engineering-guided development (e.g., dams and levees) [85]. Other approaches aimed at risk reduction are also possible, including rezoning to reduce new risk or buyouts within existing high-risk areas [86].

The results of this work show variability within streamflow and system response patterns in future simulations under RCP 8.5 for the two models considered (GFDL and CCSM). Based on the results, the seasonality of future streamflow is expected to lengthen in the future, leading to earlier snowmelt events in the spring and later streamflow events in the late fall. This impact is primarily influenced by the extension of warm seasons, where above-freezing air temperatures support streamflow for longer periods throughout the year. This coincides with a decrease in the snow season length as warm season lengths extend both earlier and later compared to the historical period, which has been identified in prior studies of the region [87]. Previous studies have also highlighted an increase in both wintertime precipitation and total year precipitation in the region over recent decades, along with an increase in extreme events [88]. While peak flow events were projected to occur in the future, the number of these events is limited, making it difficult to ascertain with high confidence how many such events could be expected. However, this result does highlight a shift from the historical period, indicating a pattern of increased variability based on the distribution of streamflow events as opposed to a semi-linear trend. While both GCMs generally aligned with the ERA simulations during the historical period after bias-correction, each simulation presented different responses when it came to mean streamflow, peak events, and total streamflow volumes in future decades. These differences in responses highlight challenges when it comes to informed planning under climate change scenarios, particularly for decision-makers hoping to plan for extreme weather events in their region. However, the approaches taken here also offer pathways toward the improved identification of plausible futures that may not otherwise have been considered under historically focused approaches and highlight a greater need for flexibility in designed solutions to address a wide range of considerations.

### 5.1. Model Limitations

While this effort helps to advance the understanding of Interior Alaska river systems under potential climate futures, it is also limited in certain applications, based on available resources, datasets, and observational data inputs, combined with the challenges of simulating an actively managed flood control project. Many of these issues are common in natural system modeling, which leads to uncertainty within modeling efforts [89]. These challenges can play an important role when exploring extreme events such as flooding, which can be particularly sensitive to non-linear responses and may require alternative approaches, such as spatial frequency analysis-derived events [90]. As GCMs are designed and tuned to consider the global-scale simulation of future climate change impacts, they are not intended to accurately represent local processes. Steps taken to guide local processes through GCM outputs may introduce added challenges for analysis. Stochasticity, model setup, and data complexity are all therefore important considerations with respect to the limitations of this work when exploring future changes in extreme events.

#### 5.1.1. Stochasticity

One of the major challenges of using reanalysis data and downscaled GCM output is the limited number of physics realizations available for many products in guiding those simulations and the computational complexity required to downscale them. Streamflow rates depend on numerous variables but are particularly responsive to short-term precipitation rates. Due to the highly variable nature of extreme hydrological events, limited realizations restrict the ability to explore parameter sensitivity more effectively under uncertain futures, with storm systems playing a particularly strong role in flood behavior in this region, such as that of the 1967 floods. However, storm systems are challenging to represent within GCMs when it comes to frequency and extent and may be highly sensitive to model mechanics and parameterizations within the GCM [91].

While the two GCMs used in this study indicated divergence in behavior, both for mean annual flow and extremes, simulations were limited to a single RCP, each with a single physics realization. Therefore, it was difficult to ascertain the level of internal model sensitivity when compared to the differences between the models themselves or between RCPs. At the time of this study, the highly limited range of GCMs considered was driven heavily by computational resource availability; thus, physical process-based downscaling across many scenarios or realizations was not possible. More recent advances in machine learning-based approaches to climate forcing may offer opportunities to improve the variability of outputs of a smaller number of physical process-based outputs in the future, offering a balance between computational efficiency and the robustness of events [92]. On the other hand, the selection of the highest RCP in this work allowed for the exploration of potential worst-case scenarios. The inclusion of a broader range of GCMs, combined with multiple physical realizations and RCPs, would allow for a greater understanding of the range of plausible future climate change responses and may produce a greater degree of confidence in the variability represented within the hydrological simulations of these systems over time.

#### 5.1.2. WRF-Hydro Model Setup

While necessary for the efficient completion of the project, choices in WRF-Hydro model design may have limited certain aspects of this modeling effort. Due to computational restrictions and data availability, forcing data were only available for three distinct time periods (2008–2017, 2038–2047, and 2068–2077). A lack of continuous data can present challenges in an environment that is also undergoing gradual changes that may impact the degree of infiltration and runoff in the region, as permafrost thaw continues to alter subsurface hydrological behavior. Because each period utilized the calibrated model parameters, each time series began with similar starting conditions, until forcing data altered those landscapes. Under natural conditions, gradual warming would occur between decades, reducing permafrost and frozen ground thickness in the region. This reduction in permafrost thickness would likely lead to an increase in groundwater storage, the infiltration of surface water, and a potential decrease in peak runoff [4]. As a result, the 20-year gap between the simulation time periods would likely produce differences in groundwater behavior that may not be present in the initial conditions for each of the simulations performed. Future work could consider the inclusion of either decadal spin-ups or a continuous series.

#### 5.1.3. Bias Variability and Uncertainty

While the outputs of the WRF-Hydro model simulations indicated extended season lengths, increasing variability, and potential shifts in high-flow occurrence and seasonality, shortcomings in forcing data due to wet bias, downscaling, and bias-correction methods led to greater uncertainty surrounding peak flows, which is expected to continue with the CMIP phase 6 models [93]. In the case of this study, monthly bias-correction of climate projections (temperature and precipitation) and the limited overlap period in datasets (2008–2017) resulted in discontinuities within monthly temperatures. While preserving annual trends, this approach resulted in jumps between months, potentially influencing rapid springtime melt events as temperature thresholds were crossed. Modified approaches for this have been shown to improve hydrological outcomes surrounding seasonal boundaries [94,95]. It is therefore possible that this resulted in an over-emphasis on spring melt events in particular, as they are highly dependent on the rate of spring warming, and peaks may be less extreme with more gradual temperature shifts between spring months.

The implementation of the WRF-Hydro model for Interior Alaska allows for future simulations to be developed to improve extreme events analyses in the region for riverine flooding. Improvements in the inclusion of permafrost dynamics, the adoption of the ERA-5 dataset for modeling, extensions of the input forcing data to longer periods to allow for improved bias-correction, and modification of the bias-correction process to include annual cycles as opposed to monthly would all be potential ways to improve future

simulation and predictive accuracy. However, despite these shortcomings, the current WRF-Hydro model outputs offer insights into changes in seasonality (both length and timing of occurrences), changes in total streamflow and summertime extremes, and perspectives into the divergence of major model outputs based on temperature/precipitation interactions.

### 5.2. Implications for Decision-Making

Watershed and flood management programs are often based on historical conditions or flood recurrence intervals. This makes adapting to rapid change or unforeseen changes challenging due to the long timelines required for policy changes, impact studies, acquiring funding, and the development of solutions. The disconnect between planning windows and environmental responses from climate change, therefore, requires an increase in forward-looking assessments of risks and attempts to understand potential shifts in extremes decades in advance. Within the study area, local governments have identified concerns surrounding the increased potential for flooding events as part of emergency management and planning efforts, with a focus on flooding, groundwater seepage, erosion and scouring events, and increasing development in the region [39]. However, the ability to plan for the future risks faced by people and built infrastructure depends on the ability to understand how those risks compare to historical events.

Globally, floods account for a significant portion of disasters, with estimates indicating that between 41 and 47 percent of disasters are caused by flood-related hazards [96,97]. As a result, the understanding of flood potential is a critical component to reducing risks in currently affected or future-affected communities. When it comes to proactive approaches to flooding, recent analyses indicate that the return on investment is high, with benefit–cost ratios for riverine flooding showing between USD 5 and 8 saved in damages for every USD 1 spent, with approaches ranging from mitigating infrastructure to improved building code requirements [98]. However, high levels of uncertainty [99], or a lack of clarity as to sources of uncertainty [89], may lead to difficulty in determining what level of proactive mitigation is justified. Simultaneously, decision-makers and planners are increasingly looking to models to identify potential local- or regional-scale challenges. Planning efforts must weigh a complex set of variables including model accuracy and uncertainty as well as socio-cultural and economic factors, including, for example, the economic resources available, the tolerance for risk in particular communities or regions, and public support. Therefore, it becomes necessary to frame outcomes in the context of the level of confidence required to undertake planning, within the scales associated with hazards.

While efforts such as this study help to provide insights for decision-makers on potential future climate change impacts, it is important to be cautious in the interpretation of the results when developing major infrastructure plans. The results of this study show agreement between the two GCMs on increasing total streamflow and season length through the study basins, but they differ in their outcomes when it comes to extreme streamflow events. This creates challenges in terms of the development of solutions, such as rezoning or the installation of large infrastructure, which may come with substantial costs or lead to the displacement of populations over time or restrictions on local land use.

Instead, general trends may inform primary concerns but must be framed within the capacity of planners to contextualize the associated uncertainty. A preference for no-regret or robust multi-hazard resilient solutions, therefore, is important in multi-decadal planning [85]. Both of these GCMs indicate the extended seasonality of streamflow; however, the GCMs also produce potentially very different futures, where streamflow extremes differ by time of year, intensity, frequency, and duration. This poses difficulties when the development of large infrastructure depends on long lead times and a significant number of resources and has the potential to generate significant ecosystem impacts. Understanding the potential for these extremes, however, provides planners with insights as to how the infrastructure designs of the past may be limited under highly uncertain futures and necessitates a potentially unforeseen need for flexibility in design.

The intent, then, is that while GCMs may not be able to highlight the future as if deterministic, the potential variability or uncertainty is communicated to the best of all abilities. This aligns with growing requirements to identify risk, scenarios, and uncertainty in applied modeling efforts [100]. From this, the outcome of this study is that, given the impacts under the two GCMs and RCP 8.5, along with the bias-correction and presence of history-exceeding events, the relative change within each GCM over time represents the potential for extreme events that exceed those that have been dealt with since the developing of flood control infrastructure within the region. While the magnitude, frequency, and duration of these events are likely to vary, this provides room to understand the potential for these events well in advance of their occurrence, helping to provide planners with insights as to how issues of awareness and preparedness can be addressed well in advance of expected extremes being realized.

### 5.3. Future Improvements

This study was limited by factors of both model and data dimensions, as well as those in the decision-making realm. Further studies may benefit from the inclusion of a broader range of RCPs and GCMs, as a limited range of scenarios may make it challenging to ascertain the full range of conditions that can be expected under future planning. A growing set of tools in the realm of machine learning may help transform these issues for extreme events [92] but may also face challenges in systems experiencing permanent state changes. While RCP 8.5 is the strongest warming scenario within CMIP5, it may not fully represent the range of flooding potential in a moderate-warming, high-precipitation future. Additionally, the assimilation of dynamic permafrost data may improve insights into seasonal flooding or extreme event potential. Beyond this, there is a need for a greater stochasticity of results to highlight where variability in short-term outputs may influence extremes. This may also be an opportunity for further exploration of bias-correction methods that could provide improved assessments of conditions within a fixed number of simulation inputs.

Another addition to this approach would be the greater inclusion of affected planners. The inclusion of regional decision-makers in the evaluation of the results would allow for improved outreach and communication efforts to ensure that similar efforts reach those assessing planning efforts. Increasing the linkages between modeling efforts and planners is an integral component of actionable change going forward due to the long timelines involved in infrastructure and planning-based mitigation and adaptation efforts. Improved linkage may also help to identify the shortcomings in operational planning that may result from incompatibilities with modeling efforts.

## 6. Conclusions

In order to better plan for the dynamic needs expected in future climate change scenarios, it is increasingly necessary to model the potential for extreme events under different climate regimes and contextualize those outputs within decision-making efforts. This study explored the potential for future hydrological system changes in three Interior Alaska rivers, assessing dynamically downscaled outputs from two GCMs under RCP 8.5. The results indicate that with the highest warming pathways, feedback responses may vary substantially between models when it comes to extreme events, based primarily on model-dependent temperature and precipitation changes. However, both GCMs agreed on long-term increases in mean and total streamflow, as well as the potential for extended streamflow season lengths in future decades. The results also indicate that as the decades progress, streamflow may exceed events that have been observed historically within these basins.

Additionally, this study highlights connections between increased seasonality and extended streamflow and the potential implications for shifts in flood control efforts. The complexity of non-stationary processes present in the study region requires greater integration between geophysical implications and disaster planning to form a comprehensive understanding of potential hazards. This research sets a foundation for future work, rec-

ognizing a need for improved data assimilation, the selection and correction of future projections, and a greater inclusion of permafrost dynamics. Through these approaches, future efforts can offer an opportunity to develop more robust and proactive adaptation strategies in systems like Interior Alaska, where significant change is already underway.

**Supplementary Materials:** The following supporting information can be downloaded at <https://www.mdpi.com/article/10.3390/w16141949/s1>: Streamflow data are provided for select forecast points and additional Figures S1–S15 provide information regarding the calibration process and selection of final parameterizations. These figures include Figure S1. Cumulative Distribution Plot of Chena River Gage, Figure S2. Cumulative Distribution Plot of Salcha River Gage, Figure S3. Cumulative Distribution Plot of Goodpaster River Gage, Figure S4. Interannual comparison of the 2014–2015 hydrologic year vs. the 2013–2012 hydrologic year for each iteration of calibration, to highlight seasonal variability, Figure S5. Comparison of highest performing iteration (blue) based on KGE scores during calibration, vs. 225 calibration iteration, Figure S6. KGE performance of calibration, by iteration, Figure S7. NSE performance of calibration, by iteration, Figure S8. Beta parameter, Figure S9. Saturated soil hydraulic conductivity, Figure S10. Lateral saturated conductivity, Figure S11. Snowmelt m parameter, Figure S12. Parameter in the surface runoff parameterization, Figure S13. Slope index, Figure S14. Maximum soil moisture for each type, and Figure S15. Bucket Height in mm.

**Author Contributions:** Conceptualization, A.P.B. and V.A.A.; methodology, A.P.B.; software, A.P.B.; validation, A.P.B., V.A.A. and P.A.B.; data curation, A.P.B. and P.A.B.; writing—original draft preparation, A.P.B.; writing—review and editing, A.P.B., V.A.A. and P.A.B.; visualization, A.P.B. and P.A.B.; funding acquisition P.A.B. and V.A.A. All authors have read and agreed to the published version of the manuscript.

**Funding:** A. Bennett and P. Bieniek were funded in part by the Strategic Environmental Research and Development Program (SERDP) through RWO 227: Aquatic Ecosystem Vulnerability to Fire and Climate Change in Alaskan Boreal Forests. Additionally, this study benefited from joint collaboration and knowledge-sharing with NOAA project NA18OAR4590417. V. Alexeev was supported by the Interdisciplinary Research for Arctic Coastal Environments (InterFACE) project through the Department of Energy, Office of Science, Biological and Environmental Research Program’s Regional and Global Model Analysis program; NOAA project NA18OAR4590417; and NSF grants 2318380 and 2040240. This work was supported in part by the high-performance computing and data storage resources operated by the Research Computing Systems (RCS) Group at the University of Alaska Fairbanks Geophysical Institute.

**Data Availability Statement:** Datasets are available upon request from the authors. Data are currently archived in University of Alaska Fairbanks Research Computing Systems (RCS) long-term storage systems. For inquiries, please contact the study authors.

**Acknowledgments:** We would like to thank our colleagues who took the time to review, comment on, and suggest revisions to this paper, particularly the dissertation committee of A. Bennett.

**Conflicts of Interest:** The authors declare no conflicts of interest. The funders had no role in the design of the study; in the collection, analyses, or interpretation of data; in the writing of the manuscript; or in the decision to publish the results.

## References

1. Walvoord, M.A.; Kurylyk, B.L. Hydrologic Impacts of Thawing Permafrost—A Review. *Vadose Zone J.* **2016**, *15*, 1–20. [[CrossRef](#)]
2. Douglas, T.A.; Turetsky, M.R.; Koven, C.D. Increased rainfall stimulates permafrost thaw across a variety of Interior Alaskan boreal ecosystems. *npj Clim. Atmos. Sci.* **2020**, *3*, 28. [[CrossRef](#)]
3. Grosse, G.; Goetz, S.; McGuire, A.D.; Romanovsky, V.E.; Schuur, E.A.G. Changing permafrost in a warming world and feedbacks to the Earth system. *Environ. Res. Lett.* **2016**, *11*, 040201. [[CrossRef](#)]
4. Jin, H.; Huang, Y.; Bense, V.F.; Ma, Q.; Marchenko, S.S.; Shepelev, V.V.; Hu, Y.; Liang, S.; Spektor, V.V.; Jin, X.; et al. Permafrost Degradation and Its Hydrogeological Impacts. *Water* **2022**, *14*, 372. [[CrossRef](#)]
5. Estimating the Magnitude and Frequency of Peak Streamflows for Ungaged Sites on Streams in Alaska and Conterminous Basins in Canada. 2003. Available online: <https://pubs.usgs.gov/wri/wri034188/> (accessed on 26 March 2024).
6. Turnipseed, D.P.; Sauer, V.B. Discharge Measurements at Gaging Stations, Chap. A8, 87. In *U.S. Geological Survey Techniques and Methods Book 3*; U.S. Geological Survey: Reston, VA, USA, 2010. Available online: <https://pubs.usgs.gov/publication/tm3A8> (accessed on 26 March 2024).

7. Legleiter, C.J.; Kinzel, P.J. Inferring Surface Flow Velocities in Sediment-Laden Alaskan Rivers from Optical Image Sequences Acquired from a Helicopter. *Remote Sens.* **2020**, *12*, 1282. [[CrossRef](#)]
8. Hodgkins, G.A. Streamflow changes in Alaska between the cool phase (1947–1976) and the warm phase (1977–2006) of the Pacific Decadal Oscillation: The influence of glaciers. *Water Resour. Res.* **2009**, *45*, 2008WR007575. [[CrossRef](#)]
9. Liao, C.; Zhuang, Q. Quantifying the Role of Snowmelt in Stream Discharge in an Alaskan Watershed: An Analysis Using a Spatially Distributed Surface Hydrology Model. *J. Geophys. Res. Earth Surf.* **2017**, *122*, 2183–2195. [[CrossRef](#)]
10. Bennett, K.E.; Cannon, A.J.; Hinzman, L. Historical trends and extremes in boreal Alaska river basins. *J. Hydrol.* **2015**, *527*, 590–607. [[CrossRef](#)]
11. Bennett, K.E.; Schwenk, J.; Bachand, C.; Gasarch, E.; Stachelek, J.; Bolton, W.R.; Rowland, J.C. Recent streamflow trends across permafrost basins of North America. *Front. Water* **2023**, *5*, 1099660. [[CrossRef](#)]
12. Cooper, M.G.; Zhou, T.; Bennett, K.E.; Bolton, W.R.; Coon, E.T.; Fleming, S.W.; Rowland, J.C.; Schwenk, J. Detecting Permafrost Active Layer Thickness Change from Nonlinear Baseflow Recession. *Water Resour. Res.* **2023**, *59*, e2022WR033154. [[CrossRef](#)]
13. Lader, R.; Walsh, J.E.; Bhatt, U.S.; Bieniek, P.A. Projections of Twenty-First-Century climate extremes for Alaska via dynamical downscaling and quantile mapping. *J. Appl. Meteorol. Climatol.* **2017**, *56*, 2393–2409. [[CrossRef](#)]
14. Gochis, D.; Barlage, M.; Cabell, R.; Dugger, A.; Fanfarillo, A.; FitzGerald, K.; McAllister, M.; McCreight, J.; RafieeiNasab, A.; Read, L.; et al. *WRF-Hydro® v5.1.1*; v5.1.1; Computer Software, Zenodo; UCAR: Boulder, CO, USA, 2020. [[CrossRef](#)]
15. Walsh, J.E.; Bhatt, U.S.; Littell, J.S.; Leonawicz, M.; Lindgren, M.; Kurkowski, T.A.; Bieniek, P.A.; Thoman, R.; Gray, S.; Rupp, T.S. Downscaling of climate model output for Alaskan stakeholders. *Environ. Model. Softw.* **2018**, *110*, 38–51. [[CrossRef](#)]
16. Bennett, K.E.; Cherry, J.E.; Balk, B.; Lindsey, S. Using MODIS estimates of fractional snow cover area to improve streamflow forecasts in interior Alaska. *Hydrol. Earth Syst. Sci.* **2019**, *23*, 2439–2459. [[CrossRef](#)]
17. Walvoord, M.A.; Striegl, R.G. Increased groundwater to stream discharge from permafrost thawing in the Yukon River basin: Potential impacts on lateral export of carbon and nitrogen. *Geophys. Res. Lett.* **2007**, *34*, 2007GL030216. [[CrossRef](#)]
18. Young, B.; Yarie, J.; Verbyla, D.; Huettmann, F.; Herrick, K.; Chapin, F.S. Modeling and mapping forest diversity in the boreal forest of interior Alaska. *Landsc. Ecol.* **2017**, *32*, 397–413. [[CrossRef](#)]
19. Mann, D.H.; Rupp, T.S.; Olson, M.A.; Duffy, P.A. Is Alaska’s Boreal Forest Now Crossing a Major Ecological Threshold? *Arct. Antarct. Alp. Res.* **2012**, *44*, 319–331. [[CrossRef](#)]
20. Wendler, G.; Shulski, M. A Century of Climate Change for Fairbanks, Alaska. *ARCTIC* **2009**, *62*, 295–300. [[CrossRef](#)]
21. Ballinger, T.J.; Bhatt, U.S.; Bieniek, P.A.; Brettschneider, B.; Lader, R.T.; Littell, J.S.; Thoman, R.L.; Waigl, C.F.; Walsh, J.E.; Webster, M.A. Alaska Terrestrial and Marine Climate Trends, 1957–2021. *J. Clim.* **2023**, *36*, 4375–4391. [[CrossRef](#)]
22. USDA Natural Resources Conservation Service. (n.d.). Upper Chena, AK (952) Precipitation Accumulation. Available online: <https://nwcc-apps.sc.egov.usda.gov/awdb/site-plots/POR/PREC/AK/Upper%20Chena.html> (accessed on 23 March 2024).
23. U.S. Census Bureau. (n.d.). QuickFacts: Fairbanks North Star Borough, Alaska. Available online: <https://www.census.gov/quickfacts/fact/table/fairbanksnorthstarboroughalaska/POP010220> (accessed on 23 March 2024).
24. U.S. Army Corps of Engineers. Moose Creek Dam Modification Study Chena River Lakes Flood Control Project North Pole, Alaska [Environmental Assessment]. 2018. Available online: <https://www.poa.usace.army.mil/Portals/34/docs/civilworks/publicreview/MCDSMREA.pdf> (accessed on 10 December 2023).
25. USGS. 5 Meter Alaska Digital Elevation Models (DEMs)—USGS National Map 3DEP Downloadable Data Collection: U.S. Geological Survey. 2022. Available online: <https://www.sciencebase.gov/catalog/item/5641fe98e4b0831b7d62e758> (accessed on 17 August 2023).
26. Childers, J.M.; Meckel, J.P.; Anderson, G.S. Floods of August 1967 in East-Central Alaska. August. 1972. Available online: <https://pubs.usgs.gov/wsp/1880a/report.pdf> (accessed on 3 September 2023).
27. Bureau of Labor and Statistics. (n.d.). CPI Inflation Calculator. Available online: <https://data.bls.gov/cgi-bin/cpicalc.pl> (accessed on 10 November 2023).
28. Flood Control Act of 1968, Pub. L. No. 90–483, 33 U.S.C. 739. 1968. Available online: <http://govinfo.gov/content/pkg/STATUTE-82/pdf/STA> (accessed on 2 March 2024).
29. U.S. Army Corps of Engineers. Overview of Tanana River Monitoring and Research Studies Near Fairbanks. Alaska. 1984. Available online: [https://archive.org/details/DTIC\\_ADA167790](https://archive.org/details/DTIC_ADA167790) (accessed on 6 November 2023).
30. Vuyovich, C.M.; Daly, S.F.; The Chena River Watershed Hydrology Model (ERDC/CRREL TR-12-1). CRREL 2012. Available online: <https://apps.dtic.mil/sti/citations/tr/ADA572119> (accessed on 10 December 2023).
31. Napolitan, Rachel. General Visits Northernmost USACE-Run Flood Control Project. U.S. Army Corps of Engineers. Available online: <https://www.usace.army.mil/Media/News-Archive/Story-Article-View/Article/2544915/general-visits-northernmost-usace-run-flood-control-project/> (accessed on 10 December 2023).
32. Glass, R.L.; Lily, M.R.; Meyer, D.F. Ground-Water Levels in an Alluvial Plain Between the Tanana and Chena Rivers Near Fairbanks, Alaska. USGS. 1996. Available online: <https://dec.alaska.gov/media/15613/gw-levels-alluvial-plain-tanana-chena.pdf> (accessed on 8 January 2024).
33. USACE. (n.d.). Innovation Leads to Productive Season for Safety Upgrade at Moose Creek Dam. Available online: <https://www.poa.usace.army.mil/Media/News-Releases/Article/3583092/innovation-leads-to-productive-season-for-safety-upgrade-at-moose-creek-dam/> (accessed on 8 January 2024).

34. U.S. Army Corps of Engineers, Fairbanks North Star Borough. Portion of Moose Creek Dam Crest Closed to Public at Chena Project > Alaska District > News Releases. U.S. Army Corps of Engineers Alaska District. Available online: <https://www.poa.usace.army.mil/Media/News-Releases/Article/3444987/joint-news-release-portion-of-moose-creek-dam-crest-closed-to-public-at-chena-p/> (accessed on 24 March 2024).
35. U.S. Army Corps of Engineers. Chena River Lakes Flood Control Project and Tanana River Levee. 2019. Available online: <https://www.poa.usace.army.mil/Portals/34/docs/operations/EFC/2019ChenaTananaOverview.pdf> (accessed on 24 March 2024).
36. Rozell, N. Fixing the Fatal Flaw of Fairbanks. Geophysical Institute. Available online: <https://www.gi.alaska.edu/alaska-science-forum/fixing-fatal-flaw-fairbanks> (accessed on 24 March 2024).
37. Pawłowski, B. Ice Jams: Causes and Effects. In *Encyclopedia of Water*, 1st ed.; Maurice, P., Ed.; Wiley: Hoboken, NJ, USA, 2019; pp. 1–9. [CrossRef]
38. Napolitan, Rachel. Ice Jams Trigger Operation of the Moose Creek Dam on Chena River. U.S. Army Corps of Engineers. Available online: <https://www.usace.army.mil/Media/News-Archive/Story-Article-View/Article/2183041/ice-jams-trigger-operation-of-the-moose-creek-dam-on-chena-river/> (accessed on 10 December 2023).
39. FNSB Emergency Management. Multi-Jurisdictional Hazard Mitigation Plan. Fairbanks North Star Borough. 2021. Available online: [https://www.fnsb.gov/DocumentCenter/View/8530/FNSB\\_MJHMP\\_Final\\_Sept2021](https://www.fnsb.gov/DocumentCenter/View/8530/FNSB_MJHMP_Final_Sept2021) (accessed on 10 December 2023).
40. Bohman, A.; Eshleman, C. Tanana, Salcha Rivers Flood Interior Alaska. Fairbanks Daily Newsminer. Available online: <https://web.archive.org/web/20080811164339/http://www.newsminer.com/news/2008/jul/31/tanana-salcha-rivers-flood-interior-alaska/> (accessed on 25 March 2024).
41. HDR, Inc. Alaska State Rail Plan—Final. 2016. Available online: <https://dot.alaska.gov/railplan/docs/Rail-Plan-Final-draft.pdf> (accessed on 25 March 2024).
42. Ellis, T. (Director). Tanana River Bridge Levee Helped Deflect Breakup Floodwaters, Residents Say. KUAC. Available online: <https://fm.kuac.org/local-news/2013-06-04/tanana-river-bridge-levee-helped-deflect-breakup-floodwaters-residents-say> (accessed on 25 March 2024).
43. USGS. (n.d.). Current Conditions for Alaska Streamflow. Available online: <https://waterdata.usgs.gov/ak/nwis/current/?type=flow> (accessed on 4 February 2024).
44. Follansbee, R. *A History of the Water Resources Branch, U.S. Geological Survey, Volume I; from Predecessor Surveys to 30 June 1919* [Report]; USGS Publications Warehouse: Reston, VA, USA, 1994. [CrossRef]
45. USGS. Chena R BL Hunts C NR Two Rivers AK. USGS Water Data for the Nation. 2023. Available online: <https://waterdata.usgs.gov/monitoring-location/15493400/> (accessed on 3 November 2023).
46. Chapter 29: Alaska. In *Fifth National Climate Assessment*; U.S. Global Change Research Program: Reston, VA, USA, 2023. [CrossRef]
47. Minsley, B.J.; Pastick, N.J.; James, S.R.; Brown, D.R.N.; Wylie, B.K.; Kass, M.A.; Romanovsky, V.E. Rapid and Gradual Permafrost Thaw: A Tale of Two Sites. *Geophys. Res. Lett.* **2022**, *49*, e2022GL100285. [CrossRef]
48. Obu, J.; Westermann, S.; Bartsch, A.; Berdnikov, N.; Christiansen, H.H.; Dashtseren, A.; Delaloye, R.; Elberling, B.; Eitzelmüller, B.; Kholodov, A.; et al. Northern Hemisphere permafrost map based on TOP modelling for 2000–2016 at 1 km<sup>2</sup> scale. *Earth-Sci. Rev.* **2019**, *193*, 299–316. [CrossRef]
49. Smith, S.L.; O’Neill, H.B.; Isaksen, K.; Noetzli, J.; Romanovsky, V.E. The changing thermal state of permafrost. *Nat. Rev. Earth Environ.* **2022**, *3*, 10–23. [CrossRef]
50. Deemy, J.B.; Takagi, K.K.; McLachlan, R.L.; Rasmussen, T.C.; Wright, S.G.; Tyler, K.N.; Garner, M.G. Hydrology, geomorphology, and soils: An overview. In *Fundamentals of Tropical Freshwater Wetlands*; Elsevier: Amsterdam, The Netherlands, 2022; pp. 43–86. [CrossRef]
51. Osetinsky-Tzidaki, I.; Fredj, E. The 50- and 100-year Exceedance Probabilities as New and Convenient Statistics for a Frequency Analysis of Extreme Events: An Example of Extreme Precipitation in Israel. *Water* **2022**, *15*, 44. [CrossRef]
52. Holmes, R.R., Jr.; Dinicola, K. *100-Year Flood—It’s All about Chance*; Report 106; General Information Product; USGS Publications Warehouse: Reston, VA, USA, 2010. [CrossRef]
53. Bird, L.J.; Bodeker, G.E.; Clem, K.R. Sensitivity of extreme precipitation to climate change inferred using artificial intelligence shows high spatial variability. *Commun. Earth Environ.* **2023**, *4*, 469. [CrossRef]
54. Vogel, R.M.; Yaindl, C.; Walter, M. Nonstationarity: Flood Magnification and Recurrence Reduction Factors in the United States: 1. Nonstationarity: Flood Magnification and Recurrence Reduction Factors in the United States. *JAWRA J. Am. Water Resour. Assoc.* **2011**, *47*, 464–474. [CrossRef]
55. IPCC. Managing the Risks of Extreme Events and Disasters to Advance Climate Change Adaptation. A Special Report of Working Groups I and II of the Intergovernmental Panel on Climate Change. In *Special Report of the Intergovernmental Panel on Climate Change*; Field, C.B., Barros, V., Stocker, T.F., Dahe, Q., Dokken, D.J., Ebi, K.L., Mastrandrea, M.D., Mach, K.J., Plattner, G.-K., Allen, S.K., et al., Eds.; Cambridge University Press: Cambridge, UK, 2012; Available online: <https://www.ipcc.ch/report/managing-the-risks-of-extreme-events-and-disasters-to-advance-climate-change-adaptation/> (accessed on 25 March 2024).
56. FEMA. 2023 National Household Survey on Disaster Preparedness. 2023. Available online: <https://fema-community-files.s3.amazonaws.com/2023-National-Household-Survey.pdf> (accessed on 8 January 2024).
57. Lechowska, E. What determines flood risk perception? A review of factors of flood risk perception and relations between its basic elements. *Nat. Hazards* **2018**, *94*, 1341–1366. [CrossRef]

58. Research Applications Laboratory. (n.d.). WRF-Hydro<sup>®</sup> Modeling System. Available online: [https://ral.ucar.edu/projects/wrf\\_hydro](https://ral.ucar.edu/projects/wrf_hydro) (accessed on 23 March 2024).
59. Gochis, D.J.; Barlage, M.; Cabell, R.; Casali, M.; Dugger, A.; FitzGerald, K.; McAllister, M.; McCreight, J.; RafieeiNasab, A.; Read, L.; et al. *The NCAR WRF-Hydro Modeling System Technical Description, Version 5.1.1*; National Center for Atmospheric Research: Boulder, CO, USA, 2020; Available online: <https://ral.ucar.edu/sites/default/files/public/WRFHydroV511TechnicalDescription.pdf> (accessed on 23 March 2024).
60. NOAA. National Water Model: Improving NOAA's Water Prediction Services. 2016. August. Available online: <https://water.noaa.gov/assets/styles/public/images/wrn-national-water-model.pdf> (accessed on 3 September 2023).
61. Farrar, M. Upgrade of National Water Model on NCEP's WCOSS System and Its Post-processing Application on the Integrated Dissemination Platform (IDP). 2023. Available online: [https://www.weather.gov/media/notification/pdf\\_2023\\_24/scn23-76\\_national\\_water\\_model\\_v3.0\\_aab.pdf](https://www.weather.gov/media/notification/pdf_2023_24/scn23-76_national_water_model_v3.0_aab.pdf) (accessed on 21 November 2023).
62. Bieniek, P.A.; Bhatt, U.S.; Walsh, J.E.; Rupp, T.S.; Zhang, J.; Krieger, J.R.; Lader, R. Dynamical downscaling of ERA-interim temperature and precipitation for Alaska. *J. Appl. Meteorol. Climatol.* **2016**, *55*, 635–654. [[CrossRef](#)]
63. Cannon, A.J.; Sobie, S.R.; Murdock, T.Q. Bias correction of GCM precipitation by quantile mapping: How well do methods preserve changes in quantiles and extremes? *J. Clim.* **2015**, *28*, 6938–6959. [[CrossRef](#)]
64. ECMWF. (n.d.). ECMWF Datasets (ERA-Interim). Available online: <https://www.ecmwf.int/en/forecasts/dataset/ecmwf-reanalysis-interim> (accessed on 6 December 2023).
65. Caswell, T.A.; Andrade, E.S.; de Lee, A.; Droettboom, M.; Hoffmann, T.; Klymak, J.; Hunter, J.; Firing, E.; Stansby, D.; Varoquaux, N.; et al. *Matplotlib/Matplotlib: REL: v3.7.2; v3.7.2*; Computer Software Zenodo; UCAR: Boulder, CO, USA, 2023. [[CrossRef](#)]
66. Harris, C.R.; Millman, K.J.; Walt, S.J. van der, Gommers, R.; Virtanen, P.; Cournapeau, D.; Wieser, E.; Taylor, J.; Berg, S.; Smith, N.J.; et al. Array programming with NumPy. *Nature* **2020**, *585*, 357–362. [[CrossRef](#)] [[PubMed](#)]
67. The Pandas Development Team. *Pandas-Dev/Pandas: Pandas, v2.0.3*; Computer Software Zenodo; UCAR: Boulder, CO, USA, 2023. [[CrossRef](#)]
68. Hoyer, S.; Roos, M.; Joseph, H.; Magin, J.; Cherian, D.; Fitzgerald, C.; Hauser, M.; Fujii, K.; Maussion, F.; Imperiale, G.; et al. *Xarray, v2023.06.0*. Computer Software Zenodo. UCAR: Boulder, CO, USA, 2023. [[CrossRef](#)]
69. Skamarock, W.; Klemp, J.; Dudhia, J.; Gill, D.; Barker, D.; Wang, W.; Huang, X.-Y.; Duda, M. *A Description of the Advanced Research WRF Version 3*; (p. 1002 KB) [Application/pdf]; UCAR/NCAR: Boulder, CO, USA, 2008. [[CrossRef](#)]
70. Taylor, K.E.; Stouffer, R.J.; Meehl, G.A. An Overview of CMIP5 and the Experiment Design. *Bull. Am. Meteorol. Soc.* **2012**, *93*, 485–498. [[CrossRef](#)]
71. Gent, P.R.; Danabasoglu, G.; Donner, L.J.; Holland, M.M.; Hunke, E.C.; Jayne, S.R.; Lawrence, D.M.; Neale, R.B.; Rasch, P.J.; Vertenstein, M.; et al. The Community Climate System Model Version 4. *J. Clim.* **2011**, *24*, 4973–4991. [[CrossRef](#)]
72. Donner, L.J.; Wyman, B.L.; Hemler, R.S.; Horowitz, L.W.; Ming, Y.; Zhao, M.; Golaz, J.-C.; Ginoux, P.; Lin, S.-J.; Schwarzkopf, M.D.; et al. The Dynamical Core, Physical Parameterizations, and Basic Simulation Characteristics of the Atmospheric Component AM3 of the GFDL Global Coupled Model CM3. *J. Clim.* **2011**, *24*, 3484–3519. [[CrossRef](#)]
73. van Vuuren, D.P.; Edmonds, J.; Kainuma, M.; Riahi, K.; Thomson, A.; Hibbard, K.; Hurtt, G.C.; Kram, T.; Krey, V.; Lamarque, J.F.; et al. The representative concentration pathways: An overview. *Clim. Chang.* **2011**, *109*, 5–31. [[CrossRef](#)]
74. Markon, C.; Gray, S.; Berman, M.; Eerkes-Medrano, L.; Hennessy, T.; Huntington, H.P.; Littell, J.; McCammon, M.; Thoman, R.; Trainor, S.F. Chapter 26: Alaska. Impacts, Risks, and Adaptation in the United States. In *The Fourth National Climate Assessment, Volume II*; U.S. Global Change Research Program: Reston, VA, USA, 2018. [[CrossRef](#)]
75. Peters, G.P.; Andrew, R.M.; Boden, T.; Canadell, J.G.; Ciais, P.; Le Quéré, C.; Marland, G.; Raupach, M.R.; Wilson, C. The challenge to keep global warming below 2 °C. *Nat. Clim. Chang.* **2013**, *3*, 4–6. [[CrossRef](#)]
76. Sampson, K.; Gochis, D. WRF Hydro GIS Pre-Processing Tools, Version 5.1.1 Documentation. 2020. Available online: [https://ral.ucar.edu/projects/wrf\\_hydro/pre-processing-tools](https://ral.ucar.edu/projects/wrf_hydro/pre-processing-tools) (accessed on 6 November 2023).
77. Aquatic Ecosystem Vulnerability to Fire and Climate Change in Alaskan Boreal Forests. (n.d.). Available online: <https://serdp-estcp.mil/projects/details/1454fd5a-c908-4a7a-8a39-2c9dfa18519d/rc18-1108-project-overview> (accessed on 4 February 2024).
78. PRISM Climate Group at Oregon State University. United States Average Annual Total Precipitation, 1991–2020 (4 km; BIL) [dataset]. 2022. Available online: <https://prism.oregonstate.edu> (accessed on 22 April 2024).
79. Logan, T.; Aoun, A.; Bourgault, P.; Dupuis, É.; Huard, D.; Lavoie, J.; Rondeau-Genesse, G.; Smith, T.J.; Alegre, R.; Barnes, C.; et al. *Ourosinclim: V0.39.0; v0.39.0*; Computer Software Zenodo; UCAR: Boulder, CO, USA, 2022. [[CrossRef](#)]
80. RafieeiNasab, A.; Dugger, A.; FitzGerald, K.; Gochis, D.; Enzinger, T.; Mazrooei, A.; McAllister, M.; Srivastava, I.; Cabell, R.; Saylor, P.; et al. Overview of WRF-Hydro Model Calibration General Strategy Optimization. Available online: [https://ral.ucar.edu/sites/default/files/public/projects/wrf-hydro/training-materials/Overview\\_of\\_Model\\_Calibration\\_Arezoo.pdf](https://ral.ucar.edu/sites/default/files/public/projects/wrf-hydro/training-materials/Overview_of_Model_Calibration_Arezoo.pdf) (accessed on 8 February 2024).
81. Mauricio Zambrano-Bigiarini. *hydroGOF: Goodness-of-Fit Functions for Comparison of Simulated and Observed Hydrological Time Series*; Version: 0.4-0; 2020; Available online: <https://zenodo.org/records/3707013> (accessed on 3 July 2024). [[CrossRef](#)]
82. Mizukami, N.; Rakovec, O.; Newman, A.J.; Clark, M.P.; Wood, A.W.; Gupta, H.V.; Kumar, R. On the choice of calibration metrics for “high-flow” estimation using hydrologic models. *Hydrol. Earth Syst. Sci.* **2019**, *23*, 2601–2614. [[CrossRef](#)]
83. Knoben, W.J.M.; Freer, J.E.; Woods, R.A. Technical note: Inherent benchmark or not? Comparing Nash-Sutcliffe and Kling-Gupta efficiency scores. *Hydrol. Earth Syst. Sci.* **2019**, *23*, 4323–4331. [[CrossRef](#)]

84. Frantzeskaki, N.; McPhearson, T.; Collier, M.J.; Kendal, D.; Bulkeley, H.; Dumitru, A.; Walsh, C.; Noble, K.; Van Wyk, E.; Ordóñez, C.; et al. Nature-Based Solutions for Urban Climate Change Adaptation: Linking Science, Policy, and Practice Communities for Evidence-Based Decision-Making. *BioScience* **2019**, *69*, 455–466. [[CrossRef](#)]
85. Stakhiv, E.Z. The centrality of engineering codes and risk-based design standards in climate adaptation strategies. *Water Policy* **2021**, *23* (Suppl. S1), 106–127. [[CrossRef](#)]
86. Chapter 31: Adaptation. In *Fifth National Climate Assessment*; U.S. Global Change Research Program: Reston, VA, USA, 2023. [[CrossRef](#)]
87. Littell, J.; McAfee, S.; Hayward, G. Alaska Snowpack Response to Climate Change: Statewide Snowfall Equivalent and Snowpack Water Scenarios. *Water* **2018**, *10*, 668. [[CrossRef](#)]
88. Druckenmiller, M.L.; Thoman, R.L.; Moon, T.A. *NOAA Arctic Report Card 2022: Executive Summary*; NOAA: Washington, DC, USA, 2022. [[CrossRef](#)]
89. Walker, W.E.; Harremoes, P.; Rotmans, J.; Van Der Sluijs, J.P.; Van Asselt, M.B.A.; Janssen, P.; Kreyer Von Krauss, M.P. Defining Uncertainty. *Integr. Assess.* **2003**, *4*, 5–17. [[CrossRef](#)]
90. Guan, T.; Liu, Y.; Sun, Z.; Zhang, J.; Chen, H.; Wang, G.; Jin, J.; Bao, Z.; Qi, W. A Framework to Identify the Uncertainty and Credibility of GCMs for Projected Future Precipitation: A Case Study in the Yellow River Basin, China. *Front. Environ. Sci.* **2022**, *10*, 863575. [[CrossRef](#)]
91. Zarzycki, C.M. Sowing Storms: How Model Timestep Can Control Tropical Cyclone Frequency in a GCM. *J. Adv. Model. Earth Syst.* **2022**, *14*, e2021MS002791. [[CrossRef](#)]
92. Leinonen, J.; Hamann, U.; Nerini, D.; Germann, U.; Franch, G. Latent diffusion models for generative precipitation nowcasting with accurate uncertainty quantification. *arXiv* **2023**, arXiv:2304.12891.
93. Lafferty, D.C.; Srivier, R.L. Downscaling and bias-correction contribute considerable uncertainty to local climate projections in CMIP6. *npj Clim. Atmos. Sci.* **2023**, *6*, 158. [[CrossRef](#)]
94. Pierce, D.W.; Cayan, D.R.; Maurer, E.P.; Abatzoglou, J.T.; Hegewisch, K.C. Improved Bias Correction Techniques for Hydrological Simulations of Climate Change. *J. Hydrometeorol.* **2015**, *16*, 2421–2442. [[CrossRef](#)]
95. Sharma, A.; Mehrotra, R.; Kusumastuti, C. Correcting systematic bias in derived hydrologic simulations—Implications for climate change assessments. *J. Water Clim. Chang.* **2023**, *14*, 2085–2102. [[CrossRef](#)]
96. Institute for Economics Peace. Ecological Threat Register 2020. Available online: [https://www.economicsandpeace.org/wp-content/uploads/2020/09/ETR\\_2020\\_web-1.pdf](https://www.economicsandpeace.org/wp-content/uploads/2020/09/ETR_2020_web-1.pdf) (accessed on 17 December 2023).
97. Centre for Research on the Epidemiology of Disasters UN Office for Disaster Risk Reduction. The Human Cost of Weather Related Disasters. 2015. Available online: <https://www.undrr.org/publication/human-cost-weather-related-disasters-1995-2015> (accessed on 20 April 2024).
98. National Institute of Building Sciences. Natural Hazard Mitigation Saves 2019 Report. 2019. Available online: [https://www.nibs.org/files/pdfs/NIBS\\_MMC\\_MitigationSaves\\_2019.pdf](https://www.nibs.org/files/pdfs/NIBS_MMC_MitigationSaves_2019.pdf) (accessed on 17 December 2023).
99. Leal Filho, W.; Stojanov, R.; Wolf, F.; Matandirotya, N.R.; Ploberger, C.; Ayal, D.Y.; Azam, F.M.S.; AL-Ahdal, T.M.A.; Sarku, R.; Tchouaffe Tchiadje, N.F.; et al. Assessing Uncertainties in Climate Change Adaptation and Land Management. *Land* **2022**, *11*, 2226. [[CrossRef](#)]
100. Department of the Interior. Applying Climate Change Science (526 DM 1; Departmental Manual). Department of the Interior. 2023. Available online: [https://www.doi.gov/sites/doi.gov/files/elips/documents/526-dm-1\\_1.pdf](https://www.doi.gov/sites/doi.gov/files/elips/documents/526-dm-1_1.pdf) (accessed on 9 February 2024).

**Disclaimer/Publisher’s Note:** The statements, opinions and data contained in all publications are solely those of the individual author(s) and contributor(s) and not of MDPI and/or the editor(s). MDPI and/or the editor(s) disclaim responsibility for any injury to people or property resulting from any ideas, methods, instructions or products referred to in the content.